Schweizerische Eidgenossenschaft
Confédération suisse
Confederazione Svizzera
Confederaziun svizra

Federal Department of the Environment, Transport, Energy and Communications DETEC

Swiss Federal Office of Energy SFOE
Energy Research and Cleantech

SWEET Call 1-2020: DeCarbCH

Deliverable report

Deliverable n°	1.1.2
Deliverable name	Data sets for renewable resources, conversion technologies and storage technologies with techno-economic and ecological information
Authors The authors bear the entire responsibility for the content of this report and for the conclusions drawn therefrom.	Chambers, Jonathan, UNIGE, Jonathan.chambers@unge.ch
Delivery date	02 2023

Table of contents

sweet swiss energy research for the energy transition

Summary

The deliverable includes data collected from the DeCarbCH project and the CROSS activity from other SWEET projects, and highlights differences in assumptions used by different groups. The data is provided on the CROSSDat platform, which allows for the hosting of datasets or the provision of metadata for datasets in other long-term archival systems. The deliverable includes data on shallow geothermal potentials, energy conversion technologies, space heating and domestic hot water, and cooling demand, which is accessible on the SWEET CROSSDat catalogue and through publications.

1 Introduction

This deliverable concerns data on renewable resources, conversion technologies and storage technologies with techno-economic and ecological information. Data was collected within DeCarbCH as well as via the related CROSS activity from other SWEET projects and collated. The work supports researchers working towards achieving the ES2050 by simplifying data collection and harmonisation. It has highlighted that there are large differences in assumptions (e.g. on costs) used by different groups and that some of the differences are due to differences in definitions that have not so far been made explicit (e.g. whether given costs for heat pumps include associated installation work, control devices, etc).

1.1 CROSSDat Platform

The data collection Task 1.1 within WP1 serves multiple needs: those of modelling in WP1, the needs of other DecarbCH work packages (as it was agreed to concentrate the data collection/aggregation within WP1) and the wider needs of the energy research community. Therefore, the data is provided on the SWEET CROSSDat platform, which allows to either host datasets or provide metadata for datasets in other long term archival systems such as Zenodo. The goal of CROSSDat is to provide an index or directory for researchers to find data on different energy topics. By focusing on the topic of energy in Switzerland it is easier to find the data needed and to contact the research group that provided it and get a better contextual understanding of its provenance. A strong collaboration was developed between WP1 and the SWEET CROSS project. The database originally envisaged in WP1 Task 1 was superseded by the broader CROSS project and delivered through the CROSSDat platform, which is continued within the SWEET COSI call and integrated inputs from various work packages. By developing the collaboration with CROSS, there was a useful synergy between the projects that avoided also building multiple unrelated energy database tools. Our discussions led to the realisation of the importance of using existing open data repositories (e.g. Zenodo) for the physical long term storage of research data outputs, while providing an index (or “database of databases”) that allowed to collect subject-specific metadata and provide a useful starting point for researchers looking for data in the energy topic. This approach was particularly successful as it was developed directly by the Early Career Researchers, Postdocs, and PhD students who are actively using and producing data and therefore have a hands-on understanding of their own needs and wants (the development was conceived around the typical “user story” of a new PhD student starting their research and needing to find relevant datasets). The approach was validated by the ongoing support of the project within COSI.

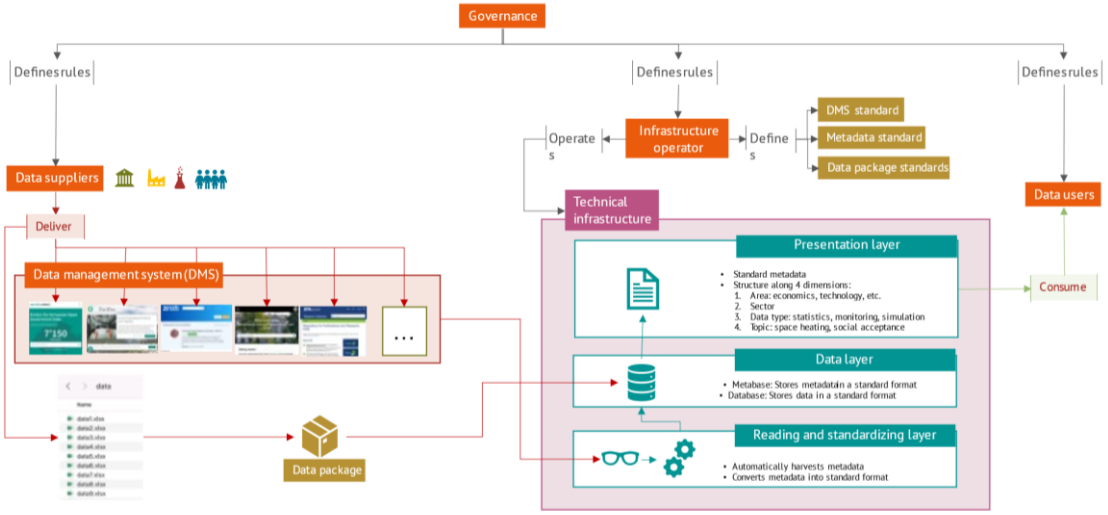

Figure 1 CROSSDat Platform overview

2 Deliverable content

The deliverable content concerns renewable resources, conversion technologies and storage technologies with techno-economic and ecological information.

2.1 CROSSDat catalogue

Data on renewable resources, conversion technologies and storage technologies has been aggregated and included in the SWEET CROSSDat catalogue (**https://sweet-cross.ch/data/**) which do-date contains 22 datasets. These cover a range of topics including energy resources, energy demands in buildings and industry, climate change projections, macroeconomic projections, and energy supplies (e.g. costs and capacities) (**Table** 1).

Table 1 CROSSDat dataset summary

Category	Number of datasets
Energy Resources	2
Energy demand in Buildings	7
Energy demand Industry	2
Energy demand other	3
Climate	2
Economics	3
Energy supply	3

2.2 Data produced in WP1

CROSSDat aggregate datasets from multiple past and current SWEET projects to meet the current needs of energy modelling. Datasets that were produced within DecarbCH and contributed to CROSSDat are summarised below.

2.2.1 Shallow geothermal potentials

Shallow geothermal potentials were developed in collaboration between UNIGE-EE and EPFL. Case study in western Switzerland found up to 87% of heat energy potentially could be supplied for DHC (Walch, Li et al. 2022). A high potential for seasonal regeneration was found. This also implies that the resources potential for shallow geothermal is not fixed but depends on the amount of (summer) thermal regeneration. Further work modelling low temperature district heating and cooling networks (LTDHC) using shallow geothermal boreholes showed that with cooling to heating ratios of between 0.4: and 1:1, such systems could be cheaper than all other options thanks to very high efficiencies and regeneration of the borehole field (Li et al. 2022) (Figure 2).

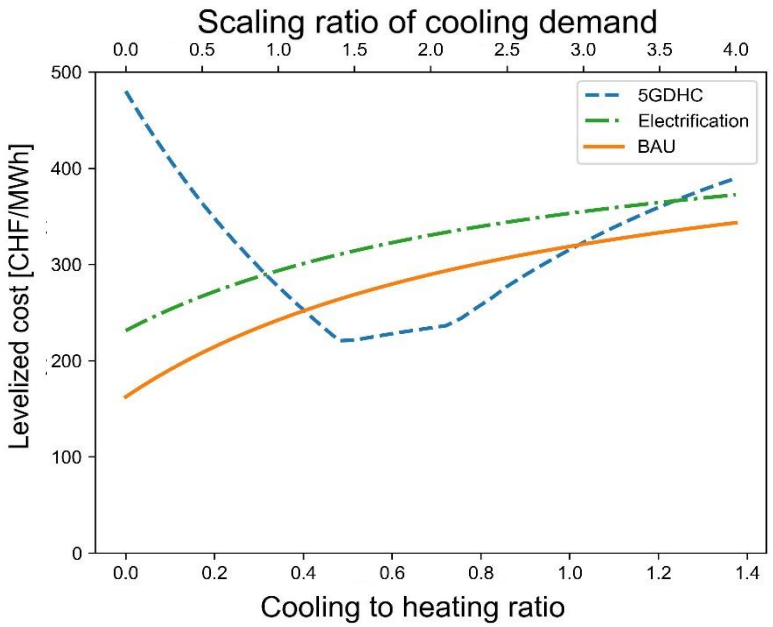

Figure 2 Levelized cost of heat for a LTDHC system as a function of cooling to heating ratio in the supplied buildings.

2.2.2 Energy conversion technologies

Data for conversion technologies (costs and efficiencies) used in Task 1.4 can be found summarised in **https://www.aramis.admin.ch/Default?DocumentID=69728**, with the key table reproduced in the Annex (**Table** 2). Common assumptions on GDP, population, energy demand, from CROSS model intercomparison activity are also used.

2.2.3 Space heating and domestic hot water

Geospatial data for space heating and domestic hot water demand in residential and service sector buildings has been published as open access. Heating demands by building typology are summarised by 4-hectare pixel (200x200m) and is accessible at **https://doi.org/10.26037/yareta:sluzlbggmjfxjj7qmyptxs7zoa**. An introduction to the data was published at the CISBAT conference (Chambers et al. 2021).

For load curves, a previously developed method for generating demand profiles has been adopted (Schneider et al. 2019). As this is a dynamic method, there is no data publication. Typical heating demand profiles for single- and multi-familiy buildings in Switzerland both with an outdated and a modern insulation standard are available on the database **https://sweet-cross.ethz.ch/data/space-heating-demand-residential-hourly-profile-hsr** .

2.2.4 Cooling demand

Cooling demand in the service sector for current reference climate (2015) and future projections for 2030 and 2050 were published as geospatial open data and are accessible at **https://doi.org/10.26037/yareta:5pdsn2n5yzesjn6xjda4w7keby**.

Cooling demand model data for residential buildings were generated using the CESAR building stock archetype simulation model (Fierz et al 2021) and published through UNIGE-EE at **https://doi.org/10.26037/yareta:tctxn4dctvdajok4vluflecgsa**.

2.2.5 Industrial demands

Industrial demand data is produced in the context of WP4 as noted in the delivery report D1.1.1. Some industry demands and process integration potentials have been published in CROSSDat, however there is a need for more detailed work per industry sector to take into account different thermal needs and temperature levels. Defining standard heating and cooling demand profiles for the industrial sector is much more complex than for the residential or service sector, since the diversity of the relevant processes is substantial. WP4 of the current project aims at enhancing the understanding of the energy demands from industry to facilitate successful integration of energy efficiency measures, and renewables within the process energy supply. The WP adopts Process Integration (PI) methodology to characterize process energy demands, aiming at both company and sectorial levels. Given the diversity of the industry sector and the challenges in obtaining publishable data that is not restricted by agreements with companies, work to produce typical industry profiles is still ongoing. For now, macro-indicators of industrial demand (estimated total demands by sectors) are used based on national reports and estimates.

3 Conclusion

The publication of datasets across many aspects of the energy system is both an important resource for researchers and reveals challenges in terms of data and assumption harmonisation. The variation between research groups also highlights the relevance of the sensitivity analysis work previously presented within WP1, which noted the large potential impacts from cost uncertainties on optimal pathways for heat electrification. This in turn raises important questions with respect to the application and interpretation of energy system models and should guide us towards parsimonious application of optimisation methods. Work ongoing in WP1 Task 1.4 addresses this at the whole energy system level by using ‘knock out’ analysis to explore what technologies appear to show most relative value, all things being equal, which allows to make use of experience gained in cost optimal models to explore future scenarios and technology potentials in a way that controls for known uncertainties in input parameters.

4 References

Chambers, J, Rittman-Frank M., Patel M. (2021) “Presentation of New Geospatial Datasets for Renewable Thermal Energy Systems Modelling in Switzerland.” Journal of Physics: Conference Series 2042 (1): 012003. **https://doi.org/10.1088/1742-6596/2042/1/012003**.

Chambers, J. (2021). “Swiss building stock heat demand data by typology, raster summary” **https://doi.org/10.26037/yareta:sluzlbggmjfxjj7qmyptxs7zoa**

Fierz L., Urban Energy Systems Lab, Empa. (2021, April 13). hues-platform/cesar-p-core: 1.3.0 (Version 1.3.0). Zenodo. **http://doi.org/10.5281/zenodo.4682881**

Li, X, and Chambers, J. (2021) “Swiss service sector cooling demand projections” **https://doi.org/10.26037/yareta:5pdsn2n5yzesjn6xjda4w7keby**.

Walch, A., Li, X., Chambers, J., Mohajeri, N., Yilmaz, S., Patel, M., & Scartezzini, J. L. (2022). Shallow geothermal energy potential for heating and cooling of buildings with regeneration under climate change scenarios. Energy, 244, 123086.

Li X, Yilmaz S, Patel MK, Chambers J. (2022) “Techno-economic analysis of fifth-generation district heating and cooling combined with seasonal borehole thermal energy storage.” Under review, Applied Energy.

Appendix 1: Data

Table 2 Assumptions on technology costs and efficiency. Energy conversion efficiency (X/Input). Reproduced from https://www.aramis.admin.ch/Default?DocumentID=69728.

Description	Investment costs	Unit	Life-time	Electr.	Thermal	Chem.	Output
Photovoltaics	500 - 1500	CHF/kWel	25	-	-	-	-
Alpine photovoltaics	2000	CHF/kWel	25	-	-	-	-
Wind power	2000	CHF/kWel	20	-	-	-	-
Regulated hydro power	6000	CHF/kWel	40	-	-	-	-
Run-of-river hydro power	6000	CHF/kWel	40	-	-	-	-
Pumped hydro storage (only pump)	1000	CHF/kWel	25	-	-	-	-
Geothermal power plant (incl. well)	10000	CHF/kWel	30	0.125	-	-	-
Gas turbine combined cycle	400 - 600	CHF/kWCH4	25	0.6	-	-	-
Gas combined heat & power plant	400 - 600	CHF/kWCH4	25	0.457	0.347	-	-
Biogas combined heat & power plant	6000	CHF/kWth	20	0.33	0.5	-	-
Small gas CHP plant	400 - 600	CHF/kWCH4	25	0.42	0.43	-	-
Wood combined heat & power plant	2000 - 3000	CHF/kWwood	25	0.164	0.676	-	-
Waste combined heat & power plant	2000 - 3000	CHF/kWwaste	25	0.119	0.663	-	-
Industrial gas burner	90	CHF/kWth	25	-	0.7	-	-
Industrial fuel burner	80	CHF/kWth	25	-	0.7	-	-
Industrial wood burner	500 - 800	CHF/kWth	25	-	0.8	-	-
Industrial waste burner	500 - 800	CHF/kWth	25	-	0.75	-	-
Industrial coal burner	500 - 800	CHF/kWth	25	-	0.8	-	-
Industrial electric heater	275	CHF/kWth	25	-	0.95	-	-
Geothermal heat generation	2000 - 4000	CHF/kWth	30	-	1	-	-
District heating heat pump	1500 - 2500	CHF/kWth	25	-	4	-	-
District heating electrical heater	325	CHF/kWth	25	-	0.95	-	-
District heating gas burner	150	CHF/kWth	25	-	0.8	-	-
District heating/industrial solar thermal	500 - 750	CHF/kWth	20	-	-	-	-
Residential air source heat pumps	2000 - 3000	CHF/kWth	25	-	3	-	-
Residential water source heat pumps	1200 - 2000	CHF/kWth	25	-	4	-	-
Residential ground source heat pumps	4000 - 6000	CHF/kWth	25	-	4	-	-
Residential electrical heater	650	CHF/kWth	25	-	0.95	-	-
Residential gas boiler	1000	CHF/kWth	25	-	0.8	-	-
Residential oil boiler	900	CHF/kWth	25	-	0.8	-	-
Residential wood boiler	950	CHF/kWth	25	-	0.8	-	-
Residential solar thermal	1200 - 1700	CHF/kWth	25	-	-	-	-
Electrolysis	600 - 1500	CHF/kWH2	25	-	-	0.7	-
Methanation process (Sabatier)	1000 - 2000	CHF/kWCH4	25	-	-	0.83	-
Gasification to methane	2000 - 3000	CHF/kWCH4	25	-	-	0.6	-
Gasification to hydrogen	3000 - 4000	CHF/kWH2	25	-	-	0.5	-

Steam methane reforming	1000 - 2000	CHF/kWH2	25	-	-	0.7	-
Pyrolysis of wood	1200	CHF/kWwood	25	-	-	0.4	-
Hydrothermal carbonization	1200	CHF/kWbiomass	25	-	-	0.4	-
Anaerobic digestion plant	1200	CHF/kWbiomass	25	-	-	0.36	-
Power-to-liquid (excl. electrolysis)	2500	CHF/kWfuel	25	-	-	0.57	-
Biomass-to-liquid	3500	CHF/kWfuel	25	-	-	0.4	-
CO_2-separation from flue gas	1800	CHF/(kg$_{CO2}$/h)	25	0.1 kWh$_{el}$/kg	1 kWh$_{el}$/kg	-	-
Direct air capture	10000	CHF/(kg$_{CO2}$/h)	25	0.4 kWh$_{el}$/kg	2 kWh$_{el}$/kg	-	-
Residential thermal energy storage	100	CHF/kWhth	25	-	-	-	0.9
Short term large thermal energy storage	10	CHF/kWhth	30	-	-	-	0.9
Seasonal thermal energy storage	0.5 - 1.5	CHF/kWhth	30	-	-	-	0.9
Battery storage	100	CHF/kWhel	20	-	-	-	0.8
Short term hydrogen storage	10 - 20	CHF/kWhH2	25	-	-	-	0.9

Appendix 2: Papers

Computers & Industrial Engineering 171 (2022) 108448

Contents lists available at ScienceDirect

Computers & Industrial Engineering

journal homepage: www.elsevier.com/locate/caie

Optimal spatial resource allocation in networks: Application to district heating and cooling

Xiang Li [a,*], Alina Walch [b], Selin Yilmaz [a], Martin Patel [a], Jonathan Chambers [a]

[a] Energy Efficiency Group, University of Geneva, Switzerland
[b] Solar Energy and Building Physics Laboratory, EPFL, Switzerland

ARTICLE INFO

Keywords:
Resource allocation
Spatial analysis
Transportation theory
Optimization

ABSTRACT

District heating and cooling networks connect and distribute thermal energy resources within a network of sources and demands. While individual networks have been extensively studied, the scaling up of this technology requires the interconnection of larger sets of networks. This poses the problem of the optimal allocation of thermal resources across a spatially distributed network. Addressing this problem guarantees the efficient utilization of thermal resources and assists achieving carbon–neutral energy systems; however, previous studies have not addressed this issue. This work contributes to filling this gap by presenting an optimal spatial allocation method combining an existing spatial clustering method, transportation theory, and linear programming to maximize the allocable resources under spatial constraints. A case study shows that the proposed method is effective at handling large-scale problems. The method enables large-scale analysis of a broad range of geo-spatially bounded resources, especially in the application of mapping renewable energy sources to supply district heating and cooling.

1. Introduction

1.1. Background

Climate change has become a global concern in the last decades. Many countries have pledged to achieve net-zero emissions in order to mitigate climate change (Internaltional Energy Agency, 2021). For instance, the European Union (EU) plans to achieve a clean and carbon neutral economy by 2050 through increased deployment of renewable energy, significant energy efficiency improvement, etc (European Commission, 2019, 2021a, 2021b). Heating and cooling play a key role in fulfilling climate commitments, as they account for 49% of global final energy consumption (International Energy Agency, 2020). Furthermore, the demand for cooling is expected to keep growing, caused by expanding demand for air conditioning due to increased frequency and intensity of heat waves under climate change, higher expected thermal comfort, higher wealth and other factors (International Energy Agency, 2018; Li et al., 2021).

Provision of heating and cooling in buildings using renewable energy sources has a high decarbonisation potential but faces a range of barriers (IRENA, IEA, and REN21, 2020). These include the higher variability of renewable energy sources, the need to connect resources with the demands, and the large range in heat supply temperature (which is higher for less efficient buildings) (Bianco et al., 2019). District heating and cooling (DHC) has been receiving increasing attention as it enables the wide use of renewables and low-temperature energy sources including solar, geothermal, waste heat, thermal energy from water bodies, etc. (Andrews et al., 2012). DHC connects multiple buildings in a district by a pipe network, allowing to supply thermal energy from central plants or distributed energy conversion units (Werner, 2017). Water is typically used as the thermal energy carrier. Advantages of DHC are firstly that it enables the integration of locally available renewable and waste energy, secondly it offers thermal energy storage which ensures flexible and reliable supply of energy, and thirdly it provides the potential to improve system energy efficiency (Rezaie and Rosen, 2012). In particular, 4th and 5th generation district heating and cooling works with a low distribution temperature of 50 °C and in the range of 0 °C to 30 °C respectively thereby allowing better integration of low-temperature renewable and waste heat sources (Buffa et al., 2019; H. Lund et al., 2014).

However, unlike fossil fuels that can be readily and very efficiently transported by freight, distributing thermal energy via water is subject to considerable thermal and pressure losses, making transporting

* Corresponding author.
E-mail address: xiang.li@unige.ch (X. Li).

https://doi.org/10.1016/j.cie.2022.108448
Received 6 August 2021; Received in revised form 9 December 2021; Accepted 8 July 2022
Available online 12 July 2022

Nomenclature

Abbreviations

DHC	District heating and cooling
EU	European Union
GIS	Geographic information system
GSHP	Ground-source heat pump
SAO	Spatial allocation with optimisation

Variables

B	Biadjacency matrix
BG	Bipartite graph
S	Set of supply nodes
D	Set of demand nodes
L	Set of links
X	Matrix representing an optimal allocation plan
η	Transportation efficiency
b	Element of biadjacency matrix
d	Capacity of demand node
i	Index of supply node
j	Index of demand node
k	Index of subgraph
m	Number of supply nodes
n	Number of demand nodes
p	Number of connected components
s	Capacity of supply node
x	Amount of resource allocated by a link
z	Allocated resources

distance a major factor that influence the system efficiency (Haiwen et al., 2010). Thermal energy, therefore, needs to be consumed within short distance from the generation site. Consequently, spatial analysis is generally conducted to map potential energy sources for DHC under the constraint of spatial proximity.

1.2. Previous studies

Many studies have focused on the national scale mapping of prospective DHC areas and low-carbon thermal energy sources (Bühler et al., 2018; R. Lund and Persson, 2016; Möller et al., 2018). In many cases where adjacent DHCs are involved, a problem arises about how to efficiently allocate identified energy sources when they are shared by several DHCs. Most studies have not treated the allocation of potential resources to DHC demands in much detail. As DHC is gaining popularity, especially in areas with dense buildings (Rismanchi, 2017), having an appropriate and accurate method to optimally allocate thermal energy for DHC should be of key importance to urban and energy system planners and engineers.

A recent study (Bühler et al., 2018) points out the issue of efficient allocation when investigating allocable energy potential of industrial excess heat, defined as the maximum amount of heat that can be allocated to district heating area under spatial constraints. This study might underestimate the allocable energy potential, since it arbitrarily assigns the excess heat sources to the nearest district heating area, which often is not the optimal assignment for full utilization of the available resource. In another study on the potential of supplying district heating networks using industrial excess heat, Chambers et al. (2020) developed a spatial clustering method that enables decomposing a national scale problem into smaller scale clusters of adjacent supplies and demands. This approach further estimates the allocable resources in clusters using a net balance method. If the total supply is lower than the total demand, then all supply is allocable. If the total supply surpasses total demand, the excess supply is curtailed, which means the allocable resources equals the total demand. It assumes that heat energy can be allocated freely within the same cluster, thus possibly overestimating the maximum usable potential.

Overall, there is a lack of studies on how to optimally allocate potential thermal energy sources to DHCs on a large scale. Inability to solve this issue will cause an inefficient use of resources. Further research is therefore needed to develop effective and accurate methods to analyse the optimal spatial allocation of resources.

1.3. Research aims and objectives

To address this research gap, we aim to develop and evaluate a method to enable optimal spatial allocation of resources applicable to DHC. The method should be scalable to handle large-scale analysis, and estimate maximum allocable resources with improved accuracy.

We propose a spatial allocation with optimisation (SAO) method that integrates geospatial data pre-processing, a graph theory-based cluster partition technique, and an optimal allocation algorithm adapted from transportation theory. We perform a case study of the shallow geothermal potential for DHC in which we demonstrate the advantage of using the SAO method when allocating thermal resources compared to a reference method without optimisation of the allocation under spatial constraints.

The strength of the SAO method lies in 1) matching between supplies and demands at high spatial resolution, 2) improving the applicability by disaggregating a large-scale problem into smaller units through graph theory, and 3) optimising the allocation of resources in a network of supplies and demands.

The scope of this work is to analyse spatial constraints in resource allocation, while the temporal aspect is not the focus. In the case study, we compute the allocation of geothermal potential for annual values. Nevertheless, when applied to resources subject to temporal constraints, for example, diurnal and seasonal variation of solar energy, the SAO method can be performed in parallel in time steps of appropriate resolution (e.g. month, day, hour).

2. Theoretical background

The investigated problem is interdisciplinary, combining existing theories from geography, engineering, mathematics, etc. Before outlining our proposed method, we first introduce two theories that provide its basis.

2.1. Graph theory

In the analysis of resource allocation, graph theory naturally arises, as it studies the pairwise relation between objects (West, 2001). Graph theory is commonly applied in real-world allocation problems like inpatient bed management (He et al., 2019), facility location problem (de Oliveira et al., 2021), etc. A graph is made up of nodes which are connected by links. In this context, potential thermal energy sources and DHC demands can be treated as nodes, while links between them (graph edges) describes connectivity.

2.1.1. Connected component

One problem of a large-scale analysis of resource allocation is the great number of objects and the following heavy computational burden. Utilizing graph partition techniques, we break down a complex large-scale problem into independent small-scale units and thus reduce the solving time of the allocation optimisation problem. A graph can be

separated into connected components. Nodes within the same connected components are connected to each other via a sequence of links (called paths), and are not connected to any other node in the rest of the graph. Two efficient algorithms exist for computing connected components of a graph which have the same running time (Dasgupta, Papadimitriou, and Vazirani, 2006): breadth-first search (Moore, 1959) and depth-first search (Hopcroft and Tarjan, 1973).

2.1.2. Bipartite graph

Bipartite graphs are mathematical models of interactions between two disjoint sets of objects, such as agencies and clients, jobs and workers. A bipartite graph is a graph which has two disjoint sets of nodes. Each link connects one node from one set and one node from the other set. Bipartite graphs are widely used for problems of optimal matching, including maximum cardinality matching, assignment problems, etc. Specifically, the assignment problem (Kuhn, 1955) shares some similarity with the resource allocation problem. It aims to find the optimal pairwise matching of nodes in a bipartite graph that minimizes the sum of weights (usually representing cost) assigned to links (Boloori Arabani and Farahani, 2012). It is solvable by integer programming. However, since the number of nodes in an assignment problem is given by an integer value and since the nodes are not dividable, the assignment problem of bipartite graphs is not directly applicable to a resources allocation problem in which supply and demand nodes have various size and are allowed to be divided. Once we drop the integrity constraints on nodes in the assignment problem, it is generalized to a transportation problem, which we illustrate in the next subsection.

2.2. Transportation theory

In mathematics and economics, the study of optimal transportation and allocation of resources is called transportation theory. The range of applications include, but are not limited to, allocation of medical resources (Sarkar et al., 2021) and humanitarian logistic (Sarma, Bera, and Das, 2019). The Hitchcock–Koopmans transportation problem (Hitchcock, 1941; Koopmans, 1942) describes a fundamental type of problem in this field. Several sources are supplying a product to numerous localities. The unit transportation costs vary with the routes between supplies and demands. It is required to find the least cost resource allocation plan that satisfies the demands from the supplies.

The original transportation problem deals with transportation cost as a linear function of delivery volume. Linear programming (Dantzig, 1963) is typically used to solve this general linear model, which is proven to be solvable in polynomial time (Khachiyan, 1979). The problem is further extended to nonlinear convex problems (Tucker, 1957) in which transportation cost is nonlinear to delivery volume, in an effort to widen the range of applications.

3. Materials and methods

3.1. Problem description

The problem introduced in Section 1.1 is to find an optimal allocation of resources to DHCs under spatial constraints. Both supplies and demands are distributed in the study area with limited connectivity. The transportation of resources is only possible via feasible connections between them. In the case of DHC, the constraint of spatial proximity applies. Transporting resources incurs losses resulting in varying transportation efficiencies of each feasible connection. The problem is then to find the optimal allocation plan between supplies and demands that maximize allocable resources.

The method to address this problem comprises the following steps:1) transformation into a graph (Section 3.2.1): convert data on supplies and demands into a bipartite graph, 2) partition (Section 3.2.2): split the original graph into subsets of connected components through graph theory, and 3) optimal allocation (Section 3.2.3): calculate the maximum allocable resources within each subset using linear programming. The method is also applicable to the optimal allocation of a range of geographically bounded resources, e.g. irrigation water and medical service.

3.2. Mathematical model

3.2.1. Transformation into a graph

We solve this problem by modelling it mathematically as a graph. When expressed as a graph, supplies and demands are treated as two independent sets of nodes of a bipartite graph. Feasible connections are identified and defined as links between supply nodes and demand nodes. The following paragraphs detail how to transform data of supplies and demands of resources into a graph.

The input data needed are the locations, geometries, and capacities of supplies and demands. Geospatial analysis is employed to identify feasible connections subject to certain criteria, for instance spatial proximity. This constraint is implemented using a cut-off distance. For each demand, all supplies for which the closest (Euclidean) distance to the demand is below the cut-off distance are connected with the demand. Once all feasible connections are identified, supplies and demands that are not connected to other objects are omitted from the analysis.

It is important to note that this method is flexible, allowing for the integration of other constraints on connecting supply and demand. Although only the constraint of spatial proximity is considered above, other constraints related to the physical properties of the network connection and transportation cost, such as flow density, pipe capacity, etc., could also be considered.

Finally, supplies are formulated as a set of nodes S. Demands are formulated as a set of nodes D. Feasible connections are formulated as a set of links L which connects a node in S to a node in D. Information on the capacity of supplies and demands is kept for further analysis. Links representing feasible connections are characterized by their length and transportation efficiency. However, information on the location and geometry are disregarded in this step. The focus is then on the pairwise connections between supplies and demands. The resulting bipartite graph $BG = (S, D, L)$ covers the whole study area.

3.2.2. Partition

Prior to performing the optimal resource allocation, the original bipartite graph BG is split into connected components based on the existence of links (connectivity of nodes) mentioned in Section 3.2.1. In the graph partition process, supply nodes S and demand nodes D are handled in the same way. Using breadth-first search, we obtain in total p connected components (so-called subgraphs), namely $BG_1, \cdots BG_p$.

Each connected component is a subset of nodes that are connected to each other by a sequence of links implying spatial proximity, but not to additional nodes outside the subset. There is no link between connected components, which implies that transporting resources between subgraphs is not possible. Therefore, we can analyse the optimal resource allocation of each subgraph separately, without introducing any error.

This has the advantage of reducing the computational cost and increasing the scalability of the method in terms of the amount of data that can be processed. This constraint on the size of the data is caused by the running time of the subsequent analysis on graphs, which tends to grow polynomially with the number of nodes. The partition into connected components limits the maximum number of nodes in each subgraph and allows each subgraph to be processed in parallel. In the case with as many parallel processes as nodes, the computation time is a function of the size of the largest single node.

3.2.3. Optimal allocation

Let an arbitrary subgraph $BG_k = (S_k, D_k, L_k)$ have m supply nodes $S_k = (S_1, \cdots, S_m)$, n demand nodes $D_k = (D_1, \cdots, D_n)$, and a set of links L_k.

Specifically, the i^{th} supply node has capacity of s_i, while the j^{th} demand node has capacity of d_j. S_i and D_j are connected if and only if L_{ij} (connecting S_i and D_j) $\in L_k$. Transporting resources via link L_{ij} is subject to the transporting efficiency of η_{ij}, which depends on the application. It is assumed that η_{ij} is not a function of the resource transported via the link.

The connectivity of the bipartite graph BG_k can be represented by a biadjacency matrix B (the adjacency matrix of a bipartite graph). Where $b_{ij} = \eta_{ij}$ if and only if $L_{ij} \in L$, and $b_{ij} = 0$ when $L_{ij} \notin L$.

An optimal allocation algorithm is introduced to accurately find the maximum allocable resources within each subgraph. The optimisation problem is formulated as a variation of the Hitchcock–Koopmans transportation problem. The total supply capacity and total demand capacity in each subgraph in our study are generally unbalanced, resulting in solving a transportation problem with surplus and deficit. Moreover, the objective of our optimisation problem is maximizing the allocation of resources, instead of minimizing the transportation cost. The mathematical formulation of the Hitchcock–Koopmans transportation problem is therefore adapted as follows:

The objective is to find an optimal allocation plan represented by matrix X in which the allocated resources z_k are maximized.

$$maximize \;\; z_k = \sum_i \sum_j b_{ij} x_{ij} \tag{1}$$

where x_{ij} is an element of X that denotes the amount of resource allocated from S_i to D_j.

The resources transported via each link must be larger than zero:

$$(i = 1, 2, \cdots, m, \;\; j = 1, 2, \cdots, n) \;\; x_{ij} \geq 0 \tag{2}$$

The allocation plan represented by matrix X is subject to the additional constraints, i.e. i) that the total resource transported from a supply must not exceed the supply capacity and ii) that the total energy transported to a demand must not exceed the demand size.

For supplies this constraint may be expressed as:

$$(i = 1, 2, \cdots, m) \;\; \sum_j x_{ij} \leq s_i \tag{3}$$

For demands this constraint may be expressed as:

$$(j = 1, 2, \cdots, n) \;\; \sum_i b_{ij} x_{ij} \leq d_j \tag{4}$$

Since the optimisation problem introduced above is linear, it can be solved using linear programming (Dantzig 1963) and is guaranteed to find the global optimal.

The total allocable resource is the sum of the maximized allocable resource of all subgraphs:

$$z_{total} = \sum_k z_k \tag{5}$$

3.3. Method implementation

The proposed method is implemented in Python 3.7. The Python library Geopandas (Jordahl, 2014) is used for spatial operations on geospatial data. The library NetworkX (Hagberg, Swart, and S Chult, 2008) is used for the creation, partition, and investigation of graphs. The linear programming library PuLP (Mitchell, OSullivan, and Dunning, 2011) is utilized to obtain the maximum allocable resources in a graph, as well as the optimal allocation plan. Other Python libraries used in this method to manipulate data include Xarray (Hoyer and Hamman, 2017), Rasterio (Gillies, Ward, and Petersen, 2013), Numpy (Walt, Colbert, and Varoquaux, 2011), and Pandas (McKinney, 2011). Table 1 summaries the functions used to implement the method.

Table 1
Python functions used in method implementation.

Step	Function	Description
Transformation into a graph	Code written by the authors using Pandas, Geopandas, Xarray, Numpy, and Rasterio	Data preparation.
	Geopandas.GeoSeries.distance	Calculate the closest distance between geospatial objects.
Partition	NetworksX.Graph	Create a graph.
	NetworkX. connected_components	Implement the breadth-first search to calculate connected components.
Optimal allocation	PuLP	Implement linear programming to solve the transportation problem. Linear programming is done via the Revised Simplex Method.

4. Case study

In this case study, the potential of geothermal energy from shallow ground-source heat pumps (GSHPs) to supply DHC is quantified in the Cantons of Vaud and Geneva (Switzerland). In the case study, potential shallow geothermal sources are spatially distributed and are required to be allocated as energy suppliers to local DHCs. The need for spatial allocation arises when there is an excess geothermal supply or a demand deficit within a DHC. Specifically, an optimal spatial allocation is required when a geothermal source is reachable by more than one DHC and the energy resource must be divided among them. We demonstrate the advantage of the SAO method by comparing it with a simpler reference method (Chambers et al., 2020), which performs spatial clustering but does not apply optimal allocation.

The input data of the case study include potential shallow geothermal supplies and potential DHC regions in the format of geographic information system (GIS) polygons. Each polygon is associated with its excess annual heating supply (for geothermal supplies) or demand deficit (for DHCs). Table 2 summarises the input data set, which is visualised in Fig. 1. It is assumed that the geothermal supplies within a cut-off distance of 1 km from DHC areas are potential heat sources. The transportation losses are ignored (transportation efficiency is set to 100%).

5. Results

In this section, we investigate the advantages of the SAO method by applying it to the case study. Section 5.1 presents the demonstration on

Table 2
Summary of the input data set of the case study.

	Data	Description	Source
Supplies	Potential shallow geothermal supplies	Geothermal sources represent the maximum energy that can be extracted from the shallow subsurface (<200 m) using closed-loop GSHP technology, without over-exploiting the heat capacity of the ground (Walch et al., 2021). This data include 4241 polygons, with in total 4187 GWh/y of excess shallow geothermal heating potential.	(Walch, 2022)
Demands	Potential DHC areas	Geographical areas for potential low-temperature district heating. This data include 291 polygons, with in total 1688 GWh/y heating demand deficit.	(Chambers et al., 2019)

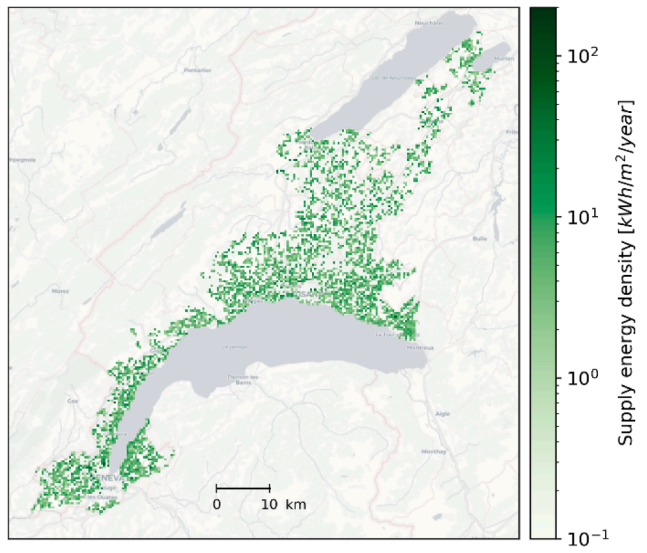

(a)

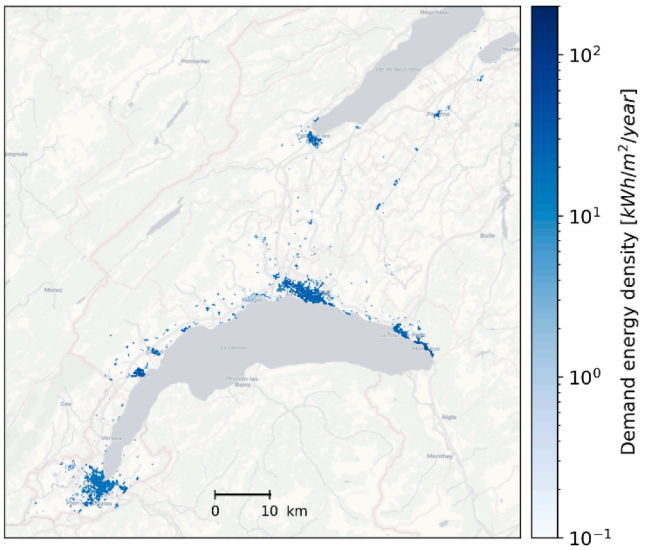

(b)

Fig. 1. Input data. (a) Potential shallow geothermal supplies and (b) district heating and cooling (DHC) areas.

large data set. Section 5.2 presents the estimated allocable geothermal energy of the SAO method in comparison with the reference method without optimisation. Section 5.3 investigates the impact of adding an optimal allocation algorithm on estimated allocable resources in an illustrative subgraph.

5.1. Demonstration on large-scale spatial allocation problem

The case study demonstrates that the SAO method can solve the spatial resource allocation problem for a large data set. Table 3 provides the change in size of the spatial resource allocation problem while applying SAO to the case study. We found that both step one (Transformation into a graph) and step two (Partition) contribute to reduce the computational burden. In step one, more than half (54%) of supply and demand nodes are omitted before creating the bipartite graph as they cannot be feasibly connected to any other node. This largely reduces the complexity of the allocation problem. In step two, the bipartite graph

Table 3
Change in size of allocation problem.

Stage	Size of allocation problem
Input data	4241 supply nodes, 291 demand nodes.
After step one - Transformation into a graph	A bipartite graph with 2077 nodes (1799 supply nodes, 278 demand nodes) and 2916 links.
After step two - Partition	In total 82 subgraphs. The biggest subgraph (in terms of number of elements) has 341 nodes (296 supply nodes, 45 demand nodes) and 578 links.

covering the whole study area is decomposed into 82 subgraphs, as shown in Fig. 2. It is apparent from Fig. 2 that the scale of the subgraphs is significantly smaller than the original bipartite graph (decreasing from a total of 2077 nodes to at most 341 nodes). The computing time required to solve the optimal allocation algorithm increases polynomially with the number of nodes. Therefore, it is almost impossible to solve the original large-scale spatial allocation problem in a reasonable time. By breaking down the complex allocation problem into smaller pieces, it becomes computationally feasible to solve the allocation for the collection of subgraphs (run time for the case study of approximately 2 min on 1 CPU).

These results indicate that the SAO method can solve large-scale spatial allocation problems. In particular, the graph partition technique used in step two contributes substantially to reducing the computational complexity while preserving a high spatial resolution.

5.2. Estimation of the allocable resources

To evaluate the performance of the SAO method in optimising the resource allocation, the results of the estimated allocable geothermal energy to DHCs in the case study, as obtained by the proposed method, is presented in comparison with a reference method without optimisation (Chambers et al., 2020). Fig. 3 compares the total allocable resources (sum of all subgraphs) of the case study estimated by the two methods, while Fig. 4 shows the subgraphs in which the two methods report different results.

The SAO method estimates that the total allocable geothermal energy is 783 GWh/y, while the reference method without optimisation

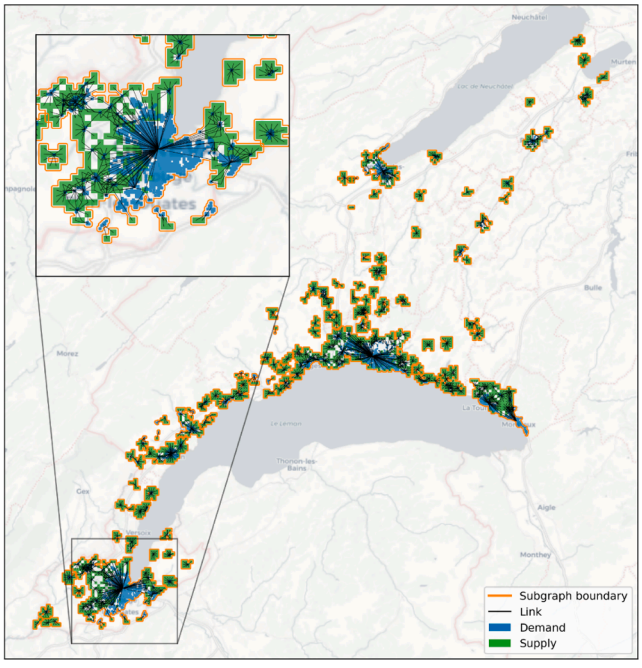

Fig. 2. Results of partition into independent subgraphs, with a zoom into the region of Geneva.

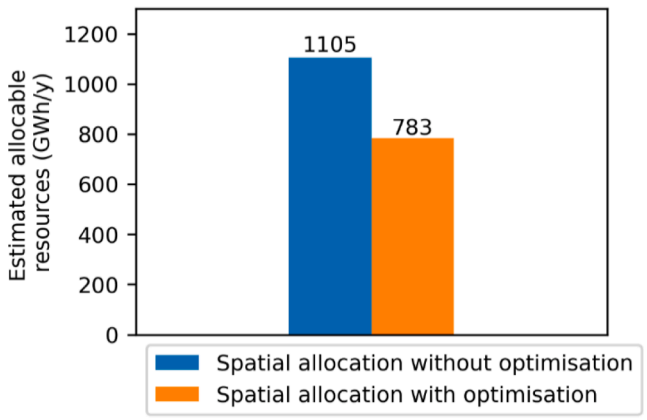

Fig. 3. Comparison of the estimated allocable resources by the spatial allocation with optimisation method and the reference method without optimisation.

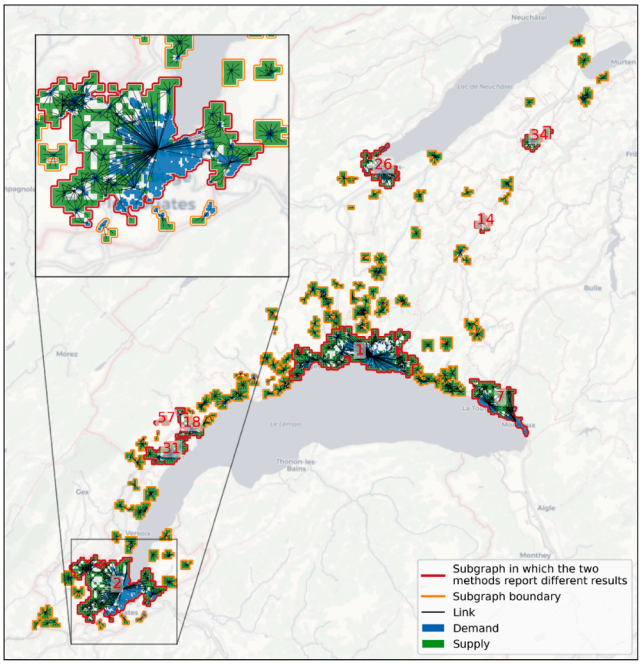

Fig. 4. Graphical representation of the difference in results between the spatial allocation optimisation methods and the reference method without optimisation, with a zoom into the region of Geneva. The numbers in red are subgraph labels.

estimates the total allocable geothermal to be 1105 GWh/y (Fig. 3). Hence, adding optimal allocation results in a significantly lower (29.1%) estimate of the total allocable geothermal potential. This is because, at the subgraph level, the SAO method always gives estimations less than or equal to the estimation obtained by the reference method. This is expected since the SAO method introduces additional constraints on the resource allocation with the subgraphs, in comparison to the reference method. There is a large range in the differences compared to the reference method (15%-45%) in 9 out of 82 subgraphs (marked in Fig. 4). In general, the differences are larger in the larger subgraphs, however this is not exclusively the case. In the remaining subgraphs, the two methods report the identical results.

5.3. Investigation of impact of SAO in illustrative subgraph

To visualise the impact of adding optimisation on the result of resource allocation, we select a single subgraph (subgraph 57, Fig. 4) as an example since there is too much data in the whole case study. Subgraph 57 has five supply nodes, two demand nodes, and six links. It covers in total 3.7 GWh/y geothermal potential supply and 4.0 GWh/y heating demand within the DHC area (Fig. 5a). The allocable geothermal energy is 3.7 GWh/y without optimisation and 2.1 GWh/y with optimisation, representing a decrease by 43%.

Without optimisation, estimating the resource allocation would possibly lead to invalid transportation of resources. Fig. 5b shows the detailed optimal allocation plan generated by the SAO method that maximise the allocable resources. In this example, although the nodes S4 and D2 could be related by a long sequence of links (S4-D1-S3-D2), the SAO method does not transport the resources along this pathway (only direct links are allowed). When such long sequences of links exist, optimising the spatial allocation is necessary to avoid an overestimation of the allocable resource.

The overestimation of allocable resources by ignoring optimal allocation also applies to other subgraphs. We found overestimation in 9 subgraphs which have at least one long sequence of links in the case study. These situations occur especially when there are relatively dense regions of supplies and demands, e.g. in the extended suburban areas around cities. Without optimisation, the allocation of resources within these extended clusters could erroneously assume that resources can be used where in reality they cannot. These results highlight the importance of intra-subgraph spatial constraints in the resource allocation problem, and demonstrate the necessary significant correction compared to the assumption that resources can be distributed freely

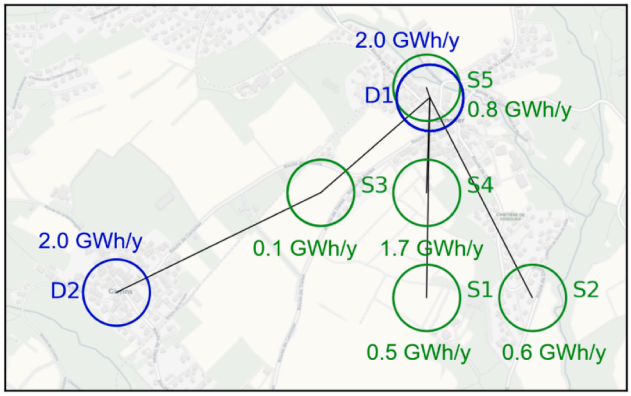

(a)

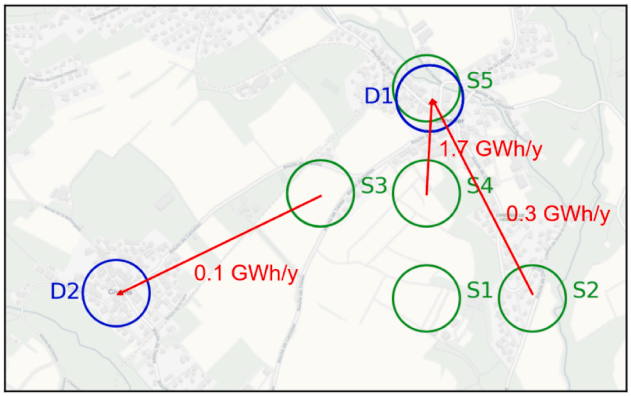

(b)

Fig. 5. Subgraph 57 (see Fig. 4) as an illustrative example of supply, demand, and links. (a) Nodes and links. The supply potential (green) and demand potential (blue) of the nodes are marked. (b) Solution of optimal allocation plan (red).

within each subgraph.

6. Discussion

This paper proposes a method combining geospatial analysis, graph theory, and transportation theory to model large-scale spatial allocation problems. The main findings and implications for policy makers, urban infrastructure designers and planners can be summarised as follows:

(1) The SAO method significantly improves the accuracy in computing allocable resources in comparison to the reference model without optimisation. We showed that the reference method without optimisation overestimates the allocable resources under spatial constraints, especially in larger subgraphs (in terms of the number of nodes) that generally account for a greater proportion of the resources to be allocated. In particular, it is common that numerous supplies and demands in close proximity form a large subgraph in dense areas such as cities. These findings suggest that it is crucial to use optimisation for spatial allocation of resources under constraints (e.g. geothermal, waste water). This allows to avoid planning errors in systems design for districts and cities.
(2) The SAO method generates an optimal resource allocation plan in addition to computing allocable resources, which is a clear advantage compared to the reference method present in literature (without optimization). Such detailed plans could be used by urban planners and engineers as a basis for planning the exploitation of resources.
(3) The computational efficiency of the SAO method allows for it to be broadly applied, due to the lower computational power needed and the potential of automated analysis.

This work is subject to several limitations. The SAO method allows to flexibly consider weights of links between supplies and demands. While fixed transportation efficiency is assigned as weights of all links in the case study, the method accepts any weights that are a linear function of transportation quantity. However, if non-linearity is included in the objective function, which is common in the real world, linear programming is not sufficient to solve the problem. In this case, nonlinear programming is necessary to extend the range of applications of the method. This is an important issue for future research. Another limitation of the method is that in the partition step, it is still possible to create subgraphs with a large quantity of nodes and links, requiring massive computing power. Further work is needed to address these computational difficulties.

7. Conclusion

This paper presents a method to estimate the maximum allocable resources in networks of supplies and demands under spatial constraints. This method for spatial allocation with optimisation (SAO) combines multidisciplinary approaches, including geospatial analysis for data processing, graph theory formulation to partition the problem into smaller scale, and an adapted Hitchcock–Koopmans transportation problem that addresses the efficient allocation of resources. We investigated the advantages of the SAO method in a regional case study of shallow geothermal potential supplying building thermal demands in the Cantons of Vaud and Geneva, Switzerland, by comparing the SAO results to a reference model without optimisation. The advantages of the SAO method include improving the accuracy in computing allocable resources compared with the reference method, and additionally providing the optimal allocation plan that maximise the resource allocation. Furthermore, we found that the method can address the spatial allocation of resources on a large scale.

The developed SAO method could be applied to the allocation of diverse geospatially bounded resources, especially in the field of mapping sources for district heating and cooling, such as industrial excess heat, geothermal energy as well as lakes and rivers as thermal reservoirs.

CRediT authorship contribution statement

Xiang Li: Conceptualization, Methodology, Software, Visualization, Writing – original draft. **Alina Walch:** Conceptualization, Data curation, Writing – review & editing. **Selin Yilmaz:** Conceptualization, Writing – review & editing, Supervision. **Martin Patel:** Writing – review & editing, Supervision, Project administration, Funding acquisition. **Jonathan Chambers:** Conceptualization, Methodology, Writing – review & editing, Supervision.

Declaration of Competing Interest

The authors declare that they have no known competing financial interests or personal relationships that could have appeared to influence the work reported in this paper.

Acknowledgements

We gratefully acknowledge financial support by the Swiss Innovation Agency Innosuisse under the project “Future Energy Efficient Buildings & Districts (SCCER- FEEB&D)”, the Chair of Energy Efficiency of University of Geneva, the project SWEET-DeCarbCH (Decarbonisation of Cooling and Heating in Switzerland, funded by the Swiss Federal Office of Energy/SFOE) and the Swiss National Science Foundation (SNSF) under the National Research Program 75 (Big Data).

References

Andrews, David et al. (2012). *Background report on EU-27 district heating and cooling potentials, barriers, best practice and measures of promotion*. https://setis.ec.europa.eu/system/files/JRCDistrictheatingandcooling.pdf.
Bianco, Emanuele et al. (2019). *Renewable energy market analysis: Southeast Europe*. International Renewable Energy Agency (IRENA).
Boloori Arabani, Alireza, & Farahani, Reza Zanjirani. (2012). Facility location dynamics: An overview of classifications and applications. Computers and Industrial Engineering 62(1): 408–20. https://doi.org/10.1016/j.cie.2011.09.018.
Buffa, Simone et al. (2019). 5th generation district heating and cooling systems: A review of existing cases in Europe. Renewable and Sustainable Energy Reviews 104(October 2018): 504–22. https://doi.org/10.1016/j.rser.2018.12.059.
Bühler, Fabian, et al. (2018). Spatiotemporal and economic analysis of industrial excess heat as a resource for district heating. *Energy, 151*, 715–728.
Chambers, Jonathan, et al. (2020). Spatiotemporal analysis of industrial excess heat supply for district heat networks in Switzerland. *Energy, 192*, Article 116705. https://doi.org/10.1016/j.energy.2019.116705
Chambers, Jonathan, Narula, Kapil, Sulzer, Matthias, & Patel, Martin K. (2019). Mapping district heating potential under evolving thermal demand scenarios and technologies: A case study for Switzerland. *Energy, 176*, 682–692. https://doi.org/10.1016/j.energy.2019.04.044
Dantzig, George B. (1963). *Linear programming and extensions*. Princeton University Press.
Dasgupta, Sanjoy, Papadimitriou, Christos, & Vazirani, Umesh. (2006). “Algorithms.”.
European Commission. (2019). European Commission *The European Green Deal*. https://eur-lex.europa.eu/legal-content/EN/TXT/PDF/?uri=CELEX:52019DC0640&from=EN.
European Commission. (2021a). Amendment to the renewable energy directive to implement the ambition of the new 2030 climate target. Brussels.
European Commission. (2021b). Angewandte Chemie International Edition, 6(11), 951–952. *Proposal for a Directive on Energy Efficiency (Recast)*. Brussels.
Gillies, Sean, Ward, B., & Petersen, A. S. (2013). Rasterio: Geospatial raster I/O for python programmers. *URL https://github. com/mapbox/rasterio*.
Hagberg, Aric, Swart, Pieter, & Chult, Daniel S. (2008). Exploring network structure, dynamics, and function using NetworkX. Los Alamos National Lab.(LANL), Los Alamos, NM (United States).
Haiwen, Shu, Lin, Duanmu, Xiangli, Li, & Yingxin, Zhu (2010). Quasi-dynamic energy-saving judgment of electric-driven seawater source heat pump district heating system over boiler house district heating system. *Energy and Buildings, 42*(12), 2424–2430. https://doi.org/10.1016/j.enbuild.2010.08.012
He, Lu et al. (2019). A systematic review of research design and modeling techniques in inpatient bed management. *Computers and Industrial Engineering* 127(April 2018): 451–66.
Hitchcock, Frank L. (1941). The distribution of a product from several sources to numerous localities. *Journal of Mathematics and Physics, 20*(1–4), 224–230. https://onlinelibrary.wiley.com/doi/epdf/10.1002/sapm1941201224.

Hopcroft, John, & Tarjan, Robert (1973). Algorithm 447: Efficient algorithms for graph manipulation. *Communications of the ACM, 16*(6), 372–378.
Hoyer, Stephan, & Hamman, Joe (2017). Xarray: ND labeled arrays and datasets in python. *Journal of Open Research Software, 5*(1).
Internaltional Energy Agency. (2021). *Net Zero by 2050*.
International Energy Agency. (2018). *The future of cooling*. Paris. www.iea.org/t&c/.
International Energy Agency. (2020). *World energy statistics and balances 2020 (database)*. Paris.
IRENA, IEA, and REN21. (2020). *Renewable energy policies in a time of transition: Heating and cooling*.
Jordahl, K. (2014). "GeoPandas: Python tools for geographic data." *URL: https://github.com/geopandas/geopandas*.
Khachiyan, Leonid Genrikhovich. (1979). A polynomial algorithm in linear programming. In *Doklady Akademii Nauk*, Russian Academy of Sciences, 1093–96.
Koopmans, Tjalling C. (1942). Exchange ratios between cargoes on various routes (non-refrigerating dry cargoes). *Memorandum for the combined shipping adjustment board, Washington DC*: 1–12.
Kuhn, Harold W. (1955). The Hungarian method for the assignment problem. *Naval Research Logistics Quarterly, 2*(1–2), 83–97.
Li, Xiang, Chambers, Jonathan, Yilmaz, Selin, & Patel, Martin K. (2021). A Monte Carlo building stock model of space cooling demand in the Swiss service sector under climate change. *Energy & Buildings, 233*. https://doi.org/10.1016/j.enbuild.2020.110662
Lund, Henrik, et al. (2014). 4th generation district heating (4GDH). Integrating smart thermal grids into future sustainable energy systems. *Energy, 68*, 1–11. https://doi.org/10.1016/j.energy.2014.02.089
Lund, Rasmus, & Persson, Urban (2016). Mapping of potential heat sources for heat pumps for district heating in Denmark. *Energy, 110*, 129–138. https://doi.org/10.1016/j.energy.2015.12.127
McKinney, Wes. (2011). "Pandas: A foundational python library for data analysis and statistics." Python for High Performance and Scientific Computing 14(9).
Mitchell, Stuart, OSullivan, Michael, & Dunning, Iain. (2011). PuLP: A linear programming toolkit for python. The University of Auckland, Auckland, New Zealand.
Möller, Bernd, et al. (2018). Heat roadmap Europe: Identifying local heat demand and supply areas with a European thermal atlas. *Energy, 158*, 281–292.
Moore, Edward F. (1959). The Shortest Path through a Maze. *In Proc. Int. Symp. Switching Theory, 1959*, 285–292.
de Oliveira, Paganini Barcellos, de Camargo, Ricardo Saraiva, de Miranda Júnior, Gilberto, & Martins Alexandre Xavier. (2021). A computational study of a decomposition approach for the dynamic two-level uncapacitated facility location problem with single and multiple allocation. Computers and Industrial Engineering 151(November 2020): 106964. https://doi.org/10.1016/j.cie.2020.106964.
Rezaie, Behnaz, & Rosen, Marc A. (2012). District heating and cooling: Review of technology and potential enhancements. *Applied Energy, 93*, 2–10. https://doi.org/10.1016/j.apenergy.2011.04.020
Rismanchi, B. (2017). District energy network (DEN), current global status and future development. Renewable and Sustainable Energy Reviews 75(July 2016): 571–79. https://doi.org/10.1016/j.rser.2016.11.025.
Sarkar, Sobhan, Pramanik, Anima, Maiti, J., & Reniers, Genserik. (2021). COVID-19 outbreak: A data-driven optimization model for allocation of patients. Computers and Industrial Engineering 161(June): 107675. https://doi.org/10.1016/j.cie.2021.107675.
Sarma, Deepshikha, Bera, Uttam Kumar, & Das, Amrit (2019). A mathematical model for resource allocation in emergency situations with the co-operation of NGOs under uncertainty. *Computers and Industrial Engineering, 137*(April), Article 106000. https://doi.org/10.1016/j.cie.2019.106000
Tucker, Albert W. (1957). "Symposium on modern techniques for extremum problems—linear and nonlinear programming." *Operations Research* 5(2): 244–57.
Walch, A., Mohajeri, N., Gudmundsson, A., & Scartezzini, J. L. (2021). Quantifying the technical geothermal potential from shallow borehole heat exchangers at regional scale. *Renewable Energy, 165*, 369–380. https://doi.org/10.1016/j.renene.2020.11.019
Walt, Stéfan van der, Chris Colbert, S., & Varoquaux, Gael. (2011). The NumPy array: A structure for efficient numerical computation. Computing in Science & Engineering 13(2): 22–30.
Walch, Alina, et al. (2022). Shallow Geothermal Energy Potential for Heating and Cooling of Buildings with Regeneration under Climate Change Scenarios. *Energy, 244*, 123086. https://doi.org/10.1016/j.energy.2021.123086
Werner, S. (2017). International review of district heating and cooling. *Energy, 137*, 617–631. https://doi.org/10.1016/j.energy.2017.04.045
West, Douglas Brent. (2001). 2 *Introduction to Graph Theory*. Prentice hall Upper Saddle River.

Energy 244 (2022) 123086

Contents lists available at ScienceDirect

Energy

journal homepage: www.elsevier.com/locate/energy

Shallow geothermal energy potential for heating and cooling of buildings with regeneration under climate change scenarios

Alina Walch [a, 1, *], Xiang Li [b, 1], Jonathan Chambers [b], Nahid Mohajeri [c], Selin Yilmaz [b], Martin Patel [b], Jean-Louis Scartezzini [a]

[a] Solar Energy and Building Physics Laboratory, EPFL, Switzerland
[b] Chair for Energy Efficiency, University of Geneva, Switzerland
[c] Institute for Environmental Design and Engineering, University College London, UK

ARTICLE INFO

Article history:
Received 22 December 2020
Received in revised form
19 October 2021
Accepted 30 December 2021
Available online 3 January 2022

Keywords:
Shallow geothermal energy
Potential estimation
Seasonal regeneration
District heating and cooling
Climate change scenarios

ABSTRACT

Shallow ground-source heat pumps (GSHPs) are a promising technology for contributing to the decarbonisation of the energy sector. In heating-dominated climates, the combined use of GSHPs for both heating and cooling increases their technical potential, defined as the maximum energy that can be exchanged with the ground, as the re-injection of excess heat from space cooling leads to a seasonal regeneration of the ground. This paper proposes a new approach to quantify the technical potential of GSHPs, accounting for effects of seasonal regeneration, and to estimate the useful energy to supply building energy demands at regional scale. The useful energy is obtained for direct heat exchange and for district heating and cooling (DHC) under several scenarios for climate change and market penetration levels of cooling systems. The case study in western Switzerland suggests that seasonal regeneration allows for annual maximum heat extraction densities above 300 kWh/m^2 at heat injection densities above 330 kWh/m^2. Results also show that GSHPs may cover up to 63% of cooling and 55% of heating demand for individual GSHPs in 2050 in Switzerland, which increases to 87% and 85% if DHC is used. The regional-scale results may serve to inform decision making on strategic areas for installing GSHPs.

1. Introduction

Shallow geothermal energy is a promising low-carbon source to meet heating and cooling demands of buildings. The most commonly used type of shallow geothermal system in many European countries, including Switzerland, are vertical ground-source heat pumps (GSHPs) [1]. These systems exchange heat with the ground through one or multiple borehole heat exchangers (BHEs) installed at depths of up to 400 m [2]. As temperatures are rising and extreme heat events are becoming more frequent due to climate change, space cooling demands may increase worldwide by up to 750% in residential buildings and 275% in commercial buildings by 2050 [3]. In heating-dominated climates such as central Europe, growing cooling demand could motivate a combined use of shallow geothermal energy for heating and cooling of buildings, using the ground as seasonal heat storage [4]. The re-injection of excess heat from space cooling to the ground hereby permits its seasonal regeneration, which reduces negative impacts of geothermal installations on the surrounding shallow subsurface [5,6]. This has two-fold benefits for the technical geothermal potential, defined as the maximum thermal energy that can be exchanged with the ground using GSHP technology. Firstly, it allows a renewable supply of cooling demand, and secondly, it increases the potential for heating.

Evaluating the potential of GSHPs with seasonal regeneration requires (i) determining the amount of excess heat available during the regeneration period, and (ii) linking the potential GSHP systems to buildings. While individual GSHPs are directly connected to a nearby building, district heating and cooling (DHC) systems allow to transport heat between areas with high geothermal potential and areas with high energy demand [7]. In particular, 4th generation DHC, also known as low-temperature district heating (LTDH), has become attractive in Europe due to improved system efficiency, ability to integrate renewable and low-temperature sources and low carbon emissions [8,9]. DHC is thus a promising technology to increase the useful geothermal potential, defined as the useful

* Corresponding author.
E-mail address: alina.walch@epfl.ch (A. Walch).
[1] Equal contribution.

https://doi.org/10.1016/j.energy.2021.123086

Nomenclature

Abbreviations

BHE	Borehole heat exchanger
CDD	Cooling degree days
COP	Coefficient of performance
D	Scenario with district heating and cooling
DH	District heating
DHC	District heating and cooling
DHS	District energy system
FC	Scenario of full cooling
GSHP	Ground-source heat pump
HDD	Heating degree days
HGSHP	Hybrid ground-source heat pump
HP	Heat pump
IPCC	The Intergovernmental Panel on Climate Change
LTDH	Low-temperature district heating
NC	Scenario of no cooling
ND	Scenario without district heating and cooling
PC	Scenario of partial cooling
RCP	Representative concentration pathway
TLM	Topographic landscape model

Variables

B	Borehole heat exchanger spacing (m)
COP_{cool}	Coefficient of performance for cooling
COP_{heat}	Coefficient of performance for heating
H	Borehole heat exchanger depth (m)
HDD_{max}	Maximum monthly HDD
CDD_{max}	Maximum monthly CDD
H_{max}	Maximum allowed drilling depth (m)
Q_{cool}	Useful potential for supplying cooling (Wh)
Q_{extr}	Technical potential for heat extraction (Wh)
Q_{field}	Annual extractable energy of BHE field (Wh)
Q_{heat}	Useful potential for supplying heat (Wh)
Q_{inj}	Injected heat (Wh)
N_B	Number of BHE in a field
R_b^*	Borehole thermal resistance (mK/W)
R_{field}	Mean thermal interference of all surrounding BHEs (mK/W)
R_{LT}	Long-term borehole thermal resistance (mK/W)
R'_{LT}	R_{LT}, weighted by annual operating time (mK/W)
R_{seas}	Seasonal maximum thermal resistance (mK/W)
R'_{seas}	R_{seas}, weighted by maximum monthly operating time (mK/W)
T_0	Ground surface temperature (°C)
T_g	Ground temperature (°C)
T_{mf}	Mean temperature of the heat carrier fluid (°C)
$T_{mf,c}$	T_{mf} in peak cooling mode (°C)
$T_{mf,h}$	T_{mf} in peak heating mode (°C)
$T_{mf,\ min}$	Minimum temperature of the heat carrier fluid (°C)
$T_{mf,\ max}$	Maximum temperature of the heat carrier fluid (°C)
α	Ground thermal diffusivity (m^2/s)
$\delta T/\delta z$	Temperature gradient in the ground (K/m)
λ	Ground thermal conductivity (W/(m·K))
d_m	Number of days in each month
q_{max}	Heat extraction power (W/m)
q_{nom}	Nominal operating power (W/m)
t_a	Number of hours in a year (8760 h)
t_{dim}	Planning horizon (year)
t_m	Number of hours in the month of maximum heating/cooling (h)
t_{nom}	Nominal operating time in heating mode (h)
$t_{op,c}$	Number of full-load cooling hours (h)
$t_{op,h}$	Number of full-load heating hours (h)
$w_{hdd,\ max}$	Weight of maximum monthly heating operation
$w_{cdd,\ max}$	Weight of maximum monthly cooling operation

energy for supplying building energy demands.

To date, many studies of the technical geothermal potential quantify the energy that may be extracted from a single installation at a given location, for example in Italy [10,11], Spain [12], Chile [13] and southern Switzerland [14]. These studies focus on the quantification of ground parameters but neglect the impact of the built environment or other GSHP systems. The built environment and its impact on the available area for installing BHEs has so far been primarily considered in studies at district scale [15,16]. However, these studies rarely account for thermal interference [17], referring to increased ground temperature changes around densely installed BHEs, which increases the environmental impact of GSHPs and reduces their technical potential [18]. Thermal interference is addressed in studies of hypothetical borehole fields [19,20] or by studying thermal plumes around existing installations [21,22]. The regional-scale effects of thermal interference and the available area for BHE installation on the technical GSHP potential have been considered in a previous study by the authors [23], which however did not consider seasonal regeneration.

Seasonal regeneration, defined as the re-injection of heat to the ground during summer, has been mentioned in city-scale studies as a possibility to increase the geothermal potential [24]. Different heat sources for seasonal regeneration of GSHPs, notably space cooling needs and solar thermal generation, are discussed and compared in Ref. [25]. Case studies of individual buildings with seasonally regenerated GSHPs, referred to as "hybrid GSHP" (HGSHP) in Ref. [4], can be found for buildings of the residential [26], service [27] or transport sector [28]. While these studies provide an indication of the potential of seasonal regeneration, the results are specific to each case study. A large-scale view of the regeneration potential is provided in some studies by comparing fictive HGSHP systems in across a number of locations, for example for 19 cities across the EU [29], 40 cities in Greece [30] or three locations in Australia [31]. A sensitivity analysis of five types of HGSHPs across several building types in North America is provided in Ref. [32]. None of these studies, however, quantify the impact of seasonal regeneration on the geothermal potential for an entire region.

Accounting for seasonal regeneration of GSHP systems requires matching the technical geothermal potential with building energy demands. Such matching has been done at building level [33], district level [17], and at city/large scale [34,35]. However, these studies have only dealt with the mapping of potential installations to nearby buildings, thus not considering the potential of district energy systems (DHS). To date, the potential of shallow geothermal energy to supply DHS has mostly been assessed for case studies of individual DHS, often focusing on the techno-economic analysis of the DHS design [36,37]. Some case studies also address the potential of combining geothermal energy with other renewables such as wind [38] and/or solar thermal energy [39,40] in DHS. The design of DHS with geothermal heat sources has also been assessed at city scale, focusing on network design rather than technical limitations of geothermal systems [41]. At regional or national scale, a spatial mapping of potential heat sources for DHS has been

provided for Denmark [42], but excludes geothermal resources. Stegnar et al. [43] have assessed the techno-economic potential of shallow geothermal energy for DHS in Slovenia, accounting for thermal interference and local ground characteristics. Of these studies, only Formhals et al. [40] consider seasonal regeneration, and no study beyond building scale quantifies the potential for supplying heating and cooling demands from GSHP systems.

To fill the above-mentioned gaps, this paper presents a novel framework to estimate the technical and useful shallow geothermal potential from GSHPs for space heating and cooling at regional scale. The proposed framework combines, for the first time, (i) the spatial mapping between building energy demands and potential GSHPs at regional scale, (ii) the analytical modelling of seasonal regeneration for GSHPs, and (iii) the optimization of heat supply for district heating and cooling (DHC). To this end, we expand the analytical model for quantifying technical geothermal potential at regional scale, proposed by Walch et al. [23], to account for bi-directional GSHP operation (heat injection and heat extraction). In this work, excess heat from space cooling is considered for heat injection, but the proposed approach can also be used for other heat sources. We further apply a graph-theory based optimization for maximising the supply of technical geothermal potential to buildings using DHC. The method is applied to a case study in the cantons of Vaud and Geneva in Switzerland, the country with the world's highest density of direct geothermal energy use per land surface [1], mostly from GSHPs [44]. Following a scenario-based approach, we obtain the technical and useful shallow geothermal potential with and without DHC, for three market penetration levels of building cooling systems and for three climate change scenarios. To the best of our knowledge, the results present the first regional-scale estimate of shallow GSHP potential that combines space heating and cooling.

2. Methods

The proposed framework for assessing the technical and useful potential of GSHPs to cover building heating and cooling demands consists of three stages, as shown in Fig. 1: First, geospatial processing is performed to match potential GSHP systems to building energy demands (Section 2.1, green boxes in Fig. 1). Second, analytical modelling is used to quantify the technical heat exchange potential for GSHP systems (Section 2.2, blue boxes in Fig. 1). The considered GSHP systems consist of vertical closed-loop BHEs, from which heat is extracted during the winter months for space heating and re-injected using excess heat from space cooling during the summer months, leading to seasonal regeneration. Third, spatial analysis is applied to optimally allocate the technical potential between individual GSHPs and DHC, yielding the useful geothermal potential (Section 2.3, orange box in Fig. 1). All modelling steps described below were implemented using the *python* programming language.

2.1. Geospatial processing

To assess the potential for ground-source heat pumps at regional scale, we use a spatial mapping approach to (i) assign the location and arrangement (i.e. spacing) of potential BHE installations and (ii) match the resulting virtual borehole fields with the building energy demand.

2.1.1. Virtual installation of GSHP systems

To assign the location and arrangement of potential BHEs, we use the estimated available areas for BHE installation provided in Ref. [23], which have been derived from parcel data. These parcels represent individual property units, from which building footprints, other built-up areas (roads, railways, traffic-related areas and leisure zones) and natural habitat that is likely unsuitable for the installation of BHEs (water bodies, forests and wetlands, protected areas) have been removed. To obtain the available areas, a buffer of 3 m has further been subtracted from parcel boundaries and building footprints, as specified in the technical norm for geothermal installations of the Swiss association of engineers and architects (SIA) [45].

On these available areas, we virtually install BHEs as rectangular grids with spacings (B) ranging from 5 m to 100 m, assuming that all available area is covered by these BHE grids. The lower boundary for B (5 m) equals the minimum distance between BHEs in a field as defined in the SIA norm [45], while the upper boundary (100 m) equals half of the maximum considered borehole depth (see Section 3.2.2). As the thermal interference between boreholes decreases logarithmically with borehole spacing [23], the simulated B follow this pattern ($B \in \{5, 7, 10, 15, 20, 25, 30, 40, 50, 70, 100\}$ m). The intersection of the BHE grids with the available area yields the individual GSHP systems, one for each parcel and for each selected spacing B.

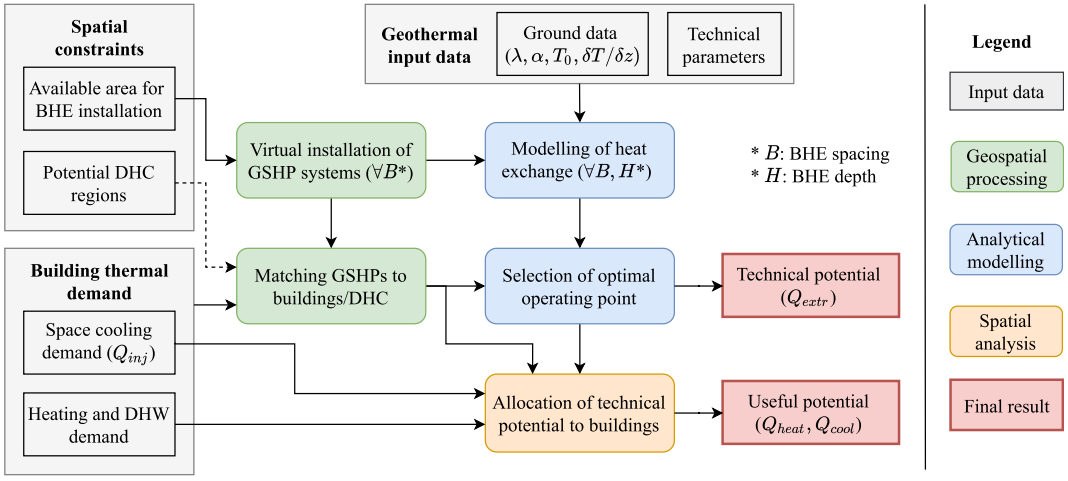

Fig. 1. Workflow for modelling the technical potential of GSHP (Q_{extr}) and the useful potential for supplying heat (Q_{heat}) and cooling (Q_{cool}), consisting of three stages: (1) Geospatial processing (green boxes), (2) Analytical modelling (blue boxes), and (3) Spatial analysis (orange box), corresponding to the following sub-sections. Dashed lines are used only if DHC is considered.

2.1.2. Matching of GSHPs to building energy demands

To match the potential GSHP systems to building energy demands, spatial constraints for the transportation of heat must be considered. In this step, we virtually connect GSHPs to buildings, for individual GSHP systems and for DHC. Generally, individual GSHPs are only connected to buildings in the same parcel, subject to land ownership. To ensure the scalability of the approach to regional scale, the matching is done for pixels of (400×400) m^2 resolution. If DHC does not exist, we hence assume that GSHPs and buildings inside the same pixel are connected. By contrast, DHC enables the connection of buildings and GSHPs with a distribution network, such that all buildings are reachable by thermal energy from GSHPs. Consequently, in areas where DHC exists, we match all GSHPs and buildings inside the same DHC and treat them as an interconnected system.

As heating demands exceed cooling demands in heating-dominated climates, the analytical model described in the following is designed to estimate the maximum heat extraction for a given amount of injected heat. Thus, the level of heat injection, here given by the space cooling demand, must be assigned to each parcel. For this, we rank all parcels within a given pixel or DHC based on their area. As the benefits of seasonal regeneration increase with the level of cooling re-injection, we re-inject the maximum possible amount of heat to the largest borehole field. If the cooling demand exceeds the maximum capacity of the largest field, cooling energy is re-injected into the second largest field and to the following parcels until all cooling demand is satisfied. This approach reduces the number of BHE fields that are used bi-directionally for heating and cooling, which is more realistic than a small heat re-injection in all fields.

2.2. Analytical modelling of heat exchange potential for bi-directional GSHPs

The proposed analytical model of bi-directional GSHPs expands upon previous work [23] to account for seasonal regeneration through the re-injection of heat to the BHEs. To this aim, a heat injection load (Q_{inj}) is added during the summer season, which reduces the long-term temperature drop in the ground. Consequently, the thermal interference between BHEs is reduced and the heat extraction potential (Q_{extr}) is increased. We further add technical limitations for heat injection and consider a higher operating time, which is typical for GSHPs with seasonal regeneration [28,46]. We focus on space cooling as heat source, but the methodology can be equally used for other sources of heat injection, such as solar thermal or industrial waste heat.

The proposed method follows a two-step approach: First, we simulate the annual extractable energy of a borehole field (Q_{field}), the maximum heat extraction power (q_{max}), and the number of full-load heating hours ($t_{op,h}$) for a range of borehole spacings B and depths H, as well as for two operating modes (nominal $t_{op,h}$ and nominal q_{max}), such as to comply with the installation standards defined in the SIA norm [45]. Second, the borehole arrangement of each GSHP system is optimised by choosing the B, H and operating mode that maximise the technical potential ($Q_{extr} + Q_{inj}$) while sustaining a feasible q_{max} and $t_{op,h}$. As the methodology is aimed at regional-scale potential analyses, it is assumed that the heat pumps of each GSHP system are well-sized to supply the estimated Q_{extr}, Q_{inj} and q_{max}. For simplification, we further assume that all systems start their operation simultaneously at time $t = 0$.

2.2.1. Modelling of heat exchange potential

The annual extractable energy of a borehole field (Q_{field}), which is simulated for each borehole arrangement (B, H), is defined as [23]:

$$Q_{field} = q_{max} \times t_{op,h} \times H \times N_B \tag{1}$$

where q_{max} is the maximum heat extraction power (in W/m) and N_B is the number of BHEs in the field. While H and N_B are assumed to be fixed for a given simulation, q_{max} and $t_{op,h}$ are free parameters that need to be selected. To assure feasible operating conditions of the GSHPs, we constrain q_{max} to at least 80% of the nominal operating power [23] and $t_{op,h}$ between the nominal operating time t_{nom} (residential heating only) [45] and the maximum operating time, which assumes that the GSHP is operated 100% of the time in the month with maximum heating load:

$$q_{max} \geq 80\%\, q_{nom} \tag{2}$$

$$t_{nom} \leq t_{op,h} \leq \frac{t_m}{w_{hdd,max}} \tag{3}$$

where t_m is the number of hours in the month of maximum heating operation.

The choices of q_{max} and $t_{op,h}$ are further constrained by the mean temperature of the heat carrier fluid inside the BHE (T_{mf}). The T_{mf} must never drop below a minimum value $T_{mf,\,min}$ in heating mode and must not exceed a maximum value $T_{mf,\,max}$ during cooling operation. Both constraints must be fulfilled at all times, from the first year to the last year of the planning horizon (t_{dim}). To simulate the heat transfer between BHE fields and the ground, we use Eskilson's analytical model [47], which represents each BHE as a finite line source. Following the principles of spatial and temporal superposition, we model the BHE operation by superimposing a long-term and a seasonal heat extraction component, as well as the thermal interference of all surrounding boreholes. The T_{mf} then equals the undisturbed ground temperature (T_g) at half the borehole depth minus the sum of the temperature drops due to each superimposed component. To avoid violating any temperature constraint, the chosen q_{max} and $t_{op,h}$ must hence fulfil the following equations for peak heat extraction (heating mode) and heat injection (cooling mode) in the first ($t = 0$) and last year ($t = t_{dim}$) of operation (cf [46,48]):

$$T_{mf,\min} \leq T_{mf,h}(t) = T_g - q_{max,h}\left(R'_{LT,h}(t) + R'_{seas,h} + R^*_b\right) + \frac{Q_{inj}}{N_B t_{op,c} H} R'_{LT,c} \tag{4}$$

$$T_{mf,max} \geq T_{mf,c}(t) = T_g + \frac{Q_{inj}}{N_B t_{op,c} H}\left(R'_{LT,c}(t) + R'_{seas,c} + R^*_b\right) - q_{max,h} R'_{LT,h} \tag{5}$$

where $T_{mf,h}$ and $T_{mf,c}$ are the T_{mf} in peak heating (h) and cooling (c) modes; Q_{inj} is the injected heat (in Wh); $t_{op,c}$ (in h) is the operating time in cooling mode; R_b^* is the borehole thermal resistance (in mK/W); R'_{LT} and R'_{seas} denote the long-term and seasonal ground thermal resistance, weighted for heating or cooling operation. At $t = 0$, we assume that $R'_{LT} = 0$. At $t = t_{dim}$, the R'_{LT} is weighted for annual mean operation, given by the fraction of operating time, and is composed of the long-term resistance of the borehole itself (R_{LT}) and the mean thermal resistance of all other BHEs within and around a field (R_{field}), which depends on B and H:

$$R'_{LT,h/c}(t) = \begin{cases} 0 & t = 0 \\ \frac{t_{op,h/c}}{t_a}\left(R_{LT}(H) + R_{field}(B,H) - R_{seas}\right) & t = t_{dim} \end{cases} \quad (6)$$

where $t_a = 8760$ h and R_{seas} is the seasonal maximum thermal resistance, which is subtracted for mathematical consistency of the model. Following [23], we model R_{LT} and R_{field} from a heat extraction pulse of duration t_{dim}, and R_{seas} from the peak of a sinusoidal heat extraction with periodicity of 1 year. The thermal resistances are functions of the ground parameters, which vary regionally (see Section 3.2.2), and the borehole geometry. R_{field} further depends on the borehole arrangement within the field, decreasing logarithmically as B increases. The mathematical formulations for R_{field}, R_{LT} and R_{seas} are provided in Ref. [23].

The R'_{seas} is the maximum monthly thermal resistance, given by multiplying R_{seas} with the fraction of the maximum monthly operating time:

$$R'_{seas,h/c} = \frac{w_{hdd/cdd,\,max}\, t_{op,h/c}}{t_m} R_{seas} \quad (7)$$

where t_m is the number of hours in the month of maximum heating/cooling operation, and $w_{hdd/cdd,\,max}$ is the weight attributed to maximum monthly operation. The weight is obtained from the heating degree days (HDD) for heating mode and from the cooling degree days (CDD) in cooling mode and allows to account for the monthly variation of the heating and cooling demand (see Appendix A). Due to the lack of a norm for cooling operation, we set $t_{op,c}$ to the maximum operating time, such that $t_{op,c} = t_m / w_{cdd,max}$ in analogy to Eq. (3).

2.2.2. Selection of optimal operating point

To select the optimal operating point of a GSHP system with a given B and H for any level of Q_{inj}, we aim to find the highest q_{max} and $t_{op,h}$ that fulfil Eqs. (2)–(5) at any time. To reduce the complexity of the selection, we consider two operating modes. The first represents a heating-only use, where $t_{op,h}$ equals the nominal value (t_{nom}, 1800–2000 h in Switzerland) [45]. We thus compute the highest q_{max} that fulfils all constraints by fixing $t_{op,h} = t_{nom}$. The second operating mode represents large installations used for both heating and cooling. These systems typically have higher operating times, around 2500–3000 h [46], while being operated at nominal power (q_{nom}). We hence fix $q_{max} = q_{nom}$ and maximise $t_{op,h}$. This second configuration is often infeasible for heating only, but it is suitable for seasonal regeneration because the long-term temperature drops around BHEs decreases as more heat is injected.

Using Eq. (1), Q_{field} is then computed for each B, H and operating mode. Out of these, the heat extraction potential of the borehole field (Q_{extr}) and the optimised borehole arrangement are obtained as the feasible solution that maximises the heat exchange potential:

$$Q_{extr} = \max_{B,H,op.\ mode} Q_{field} + Q_{inj} \quad \text{subject to Eqs. (2)} - (5)\ \forall t, H \le H_{max} \quad (8)$$

where H_{max} represents the maximum allowed drilling depth (see Section 3.2.1).

To obtain the heating (Q_{heat}) and cooling (Q_{cool}) energy exchanged with the buildings from Q_{extr} and Q_{inj}, the coefficient of performance (COP) of the heat pumps (HP) must be taken into account. We model the GSHPs as water-to-water heat pumps, which are prevalent in DHC [49]. Expecting a small increase in future HP performance compared to current COPs [50,51], we choose a constant COP for heating (COP_{heat}) as 4.5 and for cooling (COP_{cool}) as 5.5, such that (cf [50]):

$$Q_{heat} = Q_{extr}\, \frac{COP_{heat}}{(COP_{heat} - 1)} \quad (9)$$

$$Q_{cool} = Q_{inj}\, \frac{COP_{cool}}{(COP_{cool} + 1)} \quad (10)$$

2.3. Spatial analysis of useful geothermal potential

Once the technical potential is modelled, we map it with building heating demand on-site, based on matching results derived in Section 2.1.2. The useful potential for heating and cooling is defined as the portion of technical potential that is smaller than or equal to the heat demand of matched buildings. The portion of technical potential that exceeds the heat demand of matched buildings is considered as surplus potential. The surplus potential is only obtained for heating, as the analytical model described in Section 2.2 always attempts to inject the maximum possible amount of cooling demand. There are also areas where technical potential is insufficient to supply building heating or cooling, which is considered as deficit.

If DHC is considered for heat distribution, we further allocate surplus potential to nearby DHC areas with a deficit, following the on-site mapping. This allows an increase in the useful potential, as DHC is usually located in dense areas with a high demand. These areas likely have insufficient technical potential to supply the demand. The allocation process is adapted from the method of Chambers et al. [52]. This allows to analyse the supply of DHC with geothermal energy in neighbouring areas, accounting for the spatial constraint that the potential energy sources need to be within a limited range of DHC. The key strength of this method is that it uses spatial analysis and graph theory to disaggregate a large-scale case into sub-clusters of supply and demand, thus expanding the applicable spatial scale. However, this previous method allocated energy by using the simple net-balance across each sub-cluster, which assumes that energy can be allocated from supplies to demands that are not directly connected. This limitation is addressed in the present study by introducing an optimization algorithm which finds the maximum allocation of supply to demand within each sub-cluster. A detailed description of the new method is presented in a methods paper accompanying this research article [53]. Fig. 2 shows an overview of the method to link surplus geothermal potential and DHC demand. It consists of the following key steps:

Step 1. Each area with surplus geothermal potential and each DHC area with a deficit are treated as the vertices of a bipartite graph. These vertices are characterized by their geometries and heating capacities (either supply surplus or deficit). We call vertices

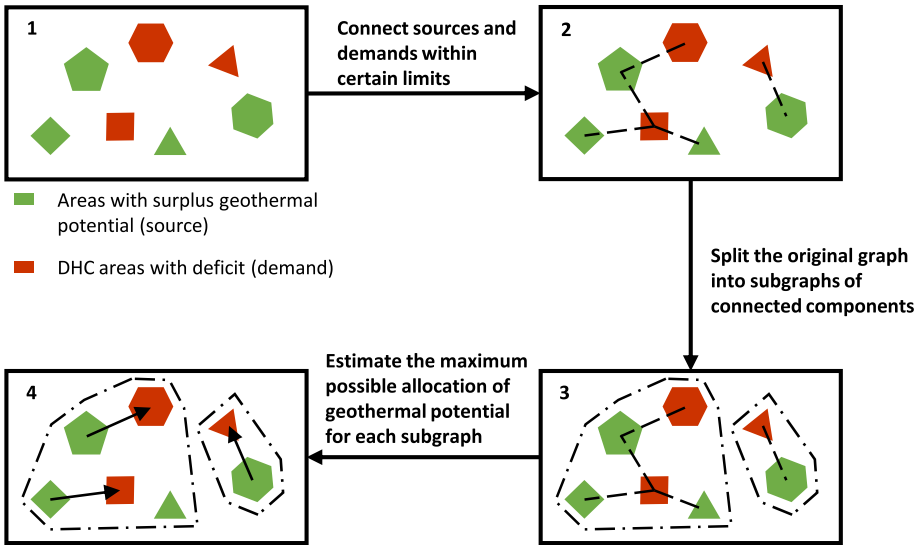

Fig. 2. Overview of the method to allocate surplus geothermal potential to district heating and cooling areas.

representing areas with surplus geothermal potential 'sources', and vertices representing DHC areas with deficit 'demand'.

Step 2. For each demand, all sources for which the closest distance to the demand is below a certain threshold are connected to the demand by an edge. To account for the variation in DHC sizes, the threshold is chosen as 20% of the length of the oriented minimum bounding box of the DHC area.

Step 3. The source/demand vertices and linking edges are converted into a large bipartite graph covering the whole study area, which is split into subgraphs of connected components (defined as a subset of vertices connected to each other, but not to any vertices outside the set).

Step 4. The maximum possible allocation of technical potential from sources to demands within each subgraph is formulated as a Hitchcock transportation problem [54] and then solved using linear programming [55].

Step 5. Finally, the maximum possible allocation of all subgraphs is summed and added to the useful potential estimated.

3. Case study

The proposed method is applied to a case study in the cantons of Vaud and Geneva in Switzerland. The case study area covers a surface of around 1600 km^2 in western Switzerland, containing two of Switzerland's largest cities (Geneva and Lausanne). The presence of high-resolution geothermal cadastres and landscape data, as well as a rapid projected growth in cooling demand [56,57], make this area highly suitable for a regional-scale study of shallow geothermal potential.

To match the technical geothermal potential with the building energy demand, we use simulated annual heating and service-sector cooling demands for the year 2050. This modelling horizon is chosen as (i) the adoption of space cooling technology is expected to increase in the coming years, and (ii) the installation of a large amount of GSHP systems would take several years. Furthermore, considering different climate change scenarios for 2050 allows to assess the robustness of the technical geothermal potential with seasonal regeneration in relation to climate change.

3.1. Scenarios considered

This work uses a scenario-based approach to assess the impact of seasonal regeneration from space cooling and the existence of DHC on the useful geothermal potential. Table 1 presents the different scenario components, namely three levels of space cooling demand, three climate change models and the possibility to use DHC. The levels of space cooling demand correspond to different penetration levels of cooling equipment in the building stock. These levels are (i) a reference case without cooling ('no cooling'), (ii) the projected penetration of cooling equipment under current tight regulation ('partial cooling'), and (iii) an extreme case saturating nearly all cooling demand ('full cooling'). The climate change models describe three representative concentration pathways (RCPs) adopted by the IPCC [58]. These are linked to the space cooling demand by modelling the diffusion of space cooling devices and the cooling intensity corresponding to each RCP. To assess the robustness of the potential estimate to climate change, we choose a stringent emission reduction scenario (RCP 2.6), an intermediate

Table 1
Description of scenario components.

Scenario components	Levels	Description
Space cooling demand	No Cooling	No space cooling demand met by GSHP (no seasonal regeneration).
	Partial Cooling	Only a portion of buildings are actively cooled. The diffusion of space cooling equipment and the growing space cooling demand is predicted based on the past trend.
	Full cooling	Extreme scenario where space cooling demand is mature and nearly saturated.
IPCC climate change models	RCP 2.6	Stringent emission reduction scenario where emissions peak around 2020 [58].
	RCP 4.5	Intermediate scenario where emissions peak around 2040 [58].
	RCP 8.5	Worst-case scenario where emissions increase throughout the 21st century [58].
DHC utilization	Without DHC	No DHC is installed (GSHPs are only connected to on-site building thermal demands).
	With DHC	In each DHC potential area, the distribution network connects all GSHPs and buildings. This allows integrating surplus geothermal potential within a limited range.

Table 2
Summary of scenario combinations.

	Climate model	Without DHC (ND)	With DHC (D)
No Cooling (NC)		Base scenario (NC-ND)	NC-D
Partial Cooling (PC)	*RCP 2.6*	PC-ND-2.6	PC-D-2.6
	RCP 4.5	PC-ND-4.5	PC-D-4.5
	RCP 8.5	PC-ND-8.5	PC-D-8.5
Full Cooling (FC)	*RCP 2.6*	FC-ND-2.6	FC-D-2.6
	RCP 4.5	FC-ND-4.5	FC-D-4.5
	RCP 8.5	FC-ND-8.5	FC-D-8.5

scenario (RCP 4.5), and a worst-case scenario (RCP 8.5). The method presented in Section 2 is applied to each combination. All scenario combinations and their naming convention used throughout the paper are shown in Table 2.

3.2. Regional datasets

Conducting a regional-scale study of geothermal potential requires the availability of high-quality data on the ground thermal properties, the building energy demand and the spatial constraints for the installation of GSHPs and the coverage of the energy demand (see Fig. 1). Table 3 provides an overview of all regional datasets and their sources.

3.2.1. Spatial constraints

Spatial constraints for the mapping of shallow GSHP potential include (i) the parcels, buildings and landscape features, required to estimate the available area for borehole installation (Section 2.1.1), (ii) potential areas for DHC (Section 2.3), and (iii) restrictions for GSHP installation (see below). The parcel boundaries are based on the official mensuration data for roughly 100,000 property units. The topographic landscape model (TLM) contains a 3D representation of various landscape objects, some of which are unsuitable for installing BHEs. A 1 m buffer is added around all unsuitable objects to account for inaccuracies of the TLM. Potential areas for low temperature district heating networks, shown in Fig. 3a, are obtained from an existing model [52]. Restrictions on the installation of GSHPs are divided into permitted, limited and prohibited zones (Fig. 3b). In permitted zones we assume a maximum drilling depth (H_{max}) of 200 m, in limited zones of 150 m, while no GSHP systems are installed in prohibited zones. These values are obtained based on typical drilling depths of existing installations in each zone, as shown in Ref. [23].

3.2.2. Geothermal input data

Estimating the technical geothermal potential (Section 2.2) requires an estimate of the long-term and seasonal thermal resistance (R_{LT}, R_{seas}), the nominal operating time ($t_{op,h}$), the seasonal load ($w_{hdd/cdd,max}$) and the nominal heat extraction rate (q_{nom}) for each borehole configuration. The borehole configurations are discretised for each parcel into 11 borehole spacings (see Section 2.1.1) and four depths, ranging from 50 m to $H_{max} = 200$ m following the spatial resolution of the ground data (Table 3). The thermal

Table 3
Overview of regional datasets.

	Dataset	Description	Resolution	Sources
Spatial constraints	Parcel boundaries	Boundaries of public & private property units	Polygons	ASIT-VD [59], SITG [60]
	Topographic Landscape Model	Incl. building footprints, other built-up areas, natural habitat	Polygons	SwissTopo [61]
	DHC zones	Potential areas for DHC	Polygons	Chambers et al. [52]
	GSHP restrictions	Permitted, limited and prohibited zones for GSHPs	Polygons	ASIT-VD [62], SITG [63]
Geothermal input data	Thermal ground properties	Thermal conductivity & diffusivity	(50×50×50) m^3 (50–300 m depth)	ASIT-VD [62], SITG [63]
	Surface temperature	Average ground surface temperature at 1 m depth	(200×200) m^2	Assouline et al. [64]
	Air temperature	Daily mean air temperature at 2 m above ground	(1×1) km^2, daily (1991–2010)	MeteoSwiss [65]
	Digital Elevation Model	Elevation map	(2×2) m^2	SwissTopo [66]
Building energy demands	Building heating demand	Space heating and domestic hot water demand	Buildings, annual	Chambers et al. [67], Schneider et al. [68]
	Building cooling demand	Building space cooling demand in the service sector	Buildings (service sector), annual	Li et al. [69]

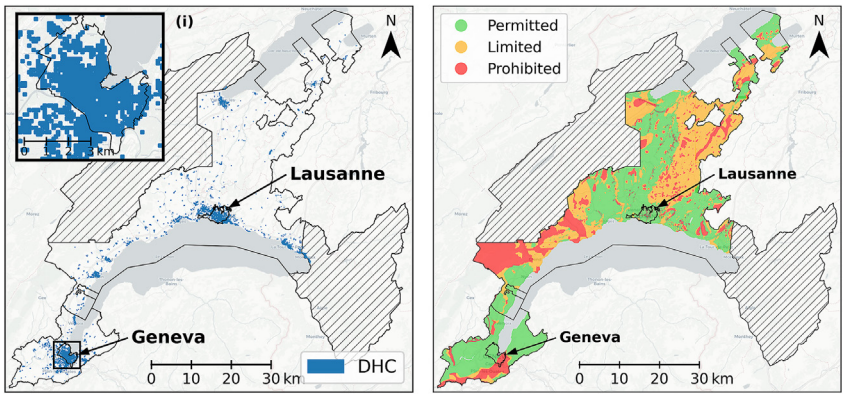

Fig. 3. Spatial constraints in the case study area in western Switzerland, a) for the potential DHC areas, and b) for the permitted areas of BHE installation. Hatched areas are not included in the case study due to a lack of available ground data.

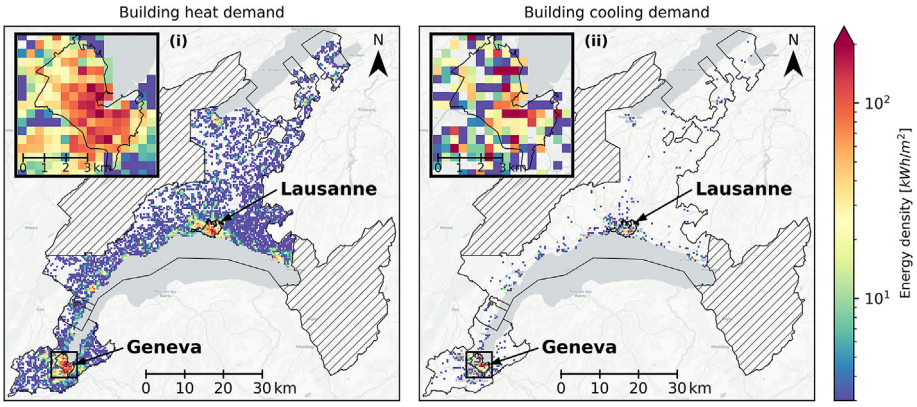

Fig. 4. Building energy demand density, a) for space heating and domestic hot water and b) for space cooling for one Monte-Carlo simulation (climate change model RCP 4.5, partial cooling). The insets (i), (ii) show the city of Geneva, Switzerland.

resistance for a dimensioning horizon of $t_{dim} = 50$ years is obtained from previous work [23], where it was derived from regional-scale data of the ground thermal conductivity (λ), diffusivity (α), the surface temperature (T_0) and the temperature gradient in the ground ($\delta T/\delta z$), which may be approximated as 0.03 K/m in the case study region [45]. The ground data is equally used to compute q_{nom} and T_g for each H based on the guidelines in the SIA norm [45]. The t_{nom} is mapped from the altitude following [45] based on a digital elevation model, assuming that it corresponds to the minimum operating time for all building types (residential and service sector). The degree days used to estimate $w_{hdd/cdd,max}$ are derived from gridded data of daily mean ambient temperature, averaged across 20 years [70]. As the data has a coarse resolution of (1×1) km^2, we spatially interpolate it to a grid of (200×200) m^2 pixels. Further technical parameters are the minimum and maximum fluid temperatures, which are set to $T_{mf,min} = -1.5°$C and $T_{mf,max} = 50°$C . These temperatures limits are chosen based on the SIA norm [45] (for $T_{mf,min}$) and existing installation examples in Switzerland [46] (for $T_{mf,max}$) such as to avoid damage of the heat exchanger tubes due to freezing or overheating.

3.2.3. Building thermal demands

An existing model was used to estimate total demand per building for heating and hot water on a yearly basis [67,68]. This is a regression-based model where typical measured heat demand intensities were linked to different building types based on the extensive metadata included in the Swiss Building Registry. A 50% reduction of demand is then applied uniformly to all building, based on the target of the Swiss Energy Strategy 2050 [71]. This 50% reduction heat demand scenario is used consistently across all scenarios, yielding the energy demand shown in Fig. 4a. In total of all buildings in the studied area, the heating demand is 6.11 TWh/y.

Table 4
Mean and 95% confidence interval of total building cooling demand in all scenarios.

	Climate model	Total building cooling demand (TWh/y)
No Cooling (NC)		0
Partial Cooling (PC)	RCP 2.6	1.33 ± 0.18
	RCP 4.5	1.57 ± 0.21
	RCP 8.5	1.82 ± 0.24
Full Cooling (FC)	RCP 2.6	2.70 ± 0.18
	RCP 4.5	3.17 ± 0.21
	RCP 8.5	3.63 ± 0.24

Building cooling demand for the partial cooling (PC) and the full cooling (FC) scenarios are generated using the Monte Carlo model introduced in the work [69]. The Monte Carlo model forecasts future building cooling demand in the service sector (e.g. offices, trade, hotels, etc.) by applying a probability distribution for the adoption of space cooling equipment in buildings, to thereby estimate the magnitude and uncertainty in the cooling demand as a function of current and future building characteristics and climate. The results are reported in Table 4 for 2000 iterations of the model. An example for a single scenario and Monte Carlo run is shown in Fig. 4b.

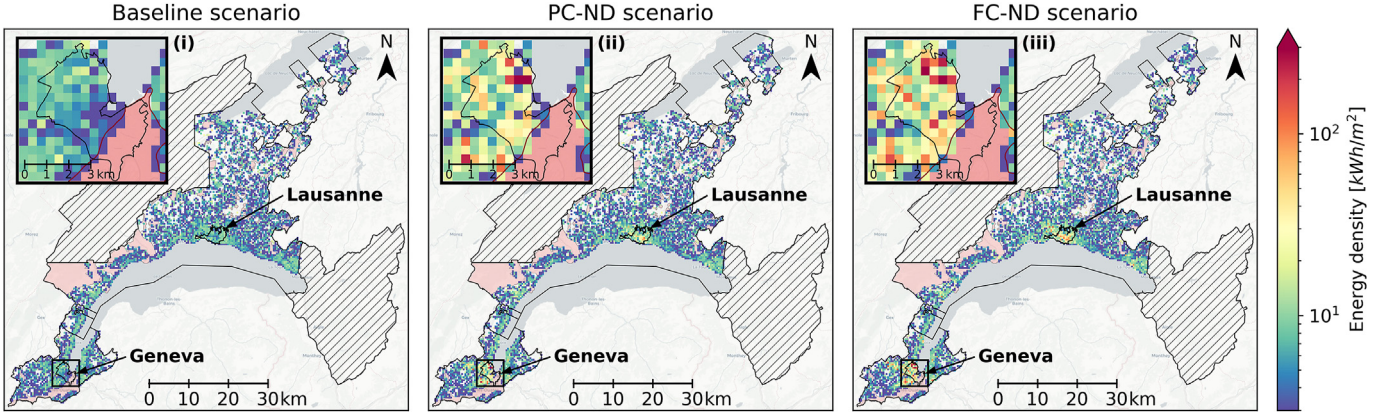

Fig. 5. Heat extraction potential (Q_{opt}) of individual GSHPs, aggregated to pixels of (400×400) m^2, for (a) baseline scenario (NC-ND), (b) partial cooling (PC-ND-4.5) and (c) full cooling scenario (FC-ND-4.5) in western Switzerland. In pink zones, GSHPs installation is prohibited.

4. Results

4.1. Impact of cooling injection on technical geothermal potential

The case study in western Switzerland shows that seasonal regeneration from the re-injection of space cooling demands increases the technical heat extraction potential (Q_{extr}) significantly. While the scenario without regeneration (NC-ND) shows a maximum annual energy density of around 15 kWh/m^2 per pixel of (400 × 400) m^2 (Fig. 5a), the maximum heat extraction density exceeds 300 kWh/m^2 in pixels with high levels of heat injection (>330 kWh/m^2), as shown in Fig. 5b and c. This 20-fold increase is explained by the strongly reduced thermal interference between boreholes, which has two-fold effects on the technical potential. Firstly, the number of boreholes increases quadratically as the average BHE spacing is reduced from B_{opt} = 20–25 m to B_{opt} = 5 – 7 m (Fig. 6a). Secondly, reduced thermal interference allows for higher operating power and time (Fig. 6b and c), which increases the heat extraction per borehole. These high energy densities are found primarily in dense urban areas, such as the city center of Geneva (see insets in Figs. 5 and 6).

In absolute terms, the technical potential can be increased by around 1 TWh if no DHC is considered (PC-ND), by 1.5 TWh with DHC (PC-D) for partial cooling, and by 2–3 TWh for full cooling (FC) (see Q_{extr} in Table 5). The results are relatively robust to different climate change scenarios, varying by ± 5% with respect to the RCP 4.5 climate model. The confidence intervals of the Monte Carlo runs vary by 5–10% for heat injection and <5% for extraction, suggesting that the total heat exchange is equally robust to the spatial distribution of cooling demand within the studied area. The scenarios further provide insights into the relation between the injected and extracted heat. As the linear fit of all scenarios (Fig. 7) shows, roughly 90% of the injected heat during summer can be extracted in winter in addition to the baseline potential of 4.6 TWh. This high conversion rate of 90% is due to the strong effect of seasonal regeneration on reducing thermal interference between boreholes.

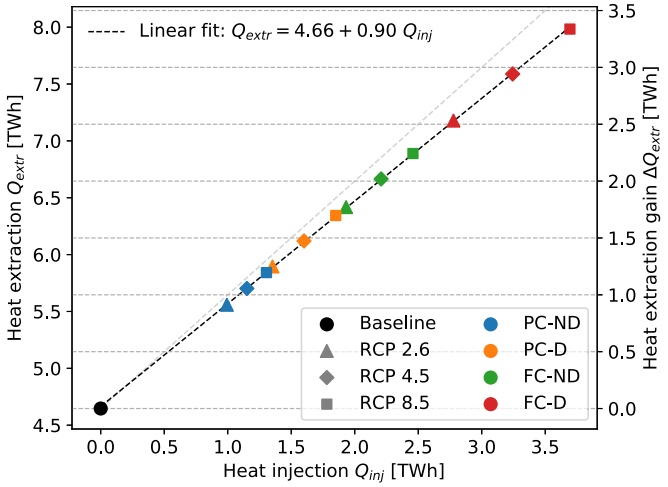

Fig. 7. Geothermal potential (Q_{extr}) as a function of injected excess heat (Q_{inj}), for all scenarios (see Table 2). The black dashed line shows the linear fit, the grey dashed line represents a slope of 1.

These results show that seasonal regeneration is essential for a sustainable large-scale deployment of GSHPs.

4.2. Supply of building heating and cooling demands

The useful potential to supply heat and cooling demand in seven scenarios of cooling penetration and climate change without DHC is presented in Table 6 and Fig. 8. Due to the spatial constraint that geothermal energy can only supply demand in a limited range from the GSHP, only a fraction of the technical potential is useful. In the base scenario (NC-ND), only 2.2 TWh of the 6.0 TWh of Q_{heat} (from 4.6 TWh of Q_{extr} provided to HPs) is useful, which would cover 35% of building heating demand. When considering seasonal regeneration from space cooling in the PC-ND scenario, 0.8–1.1 TWh of

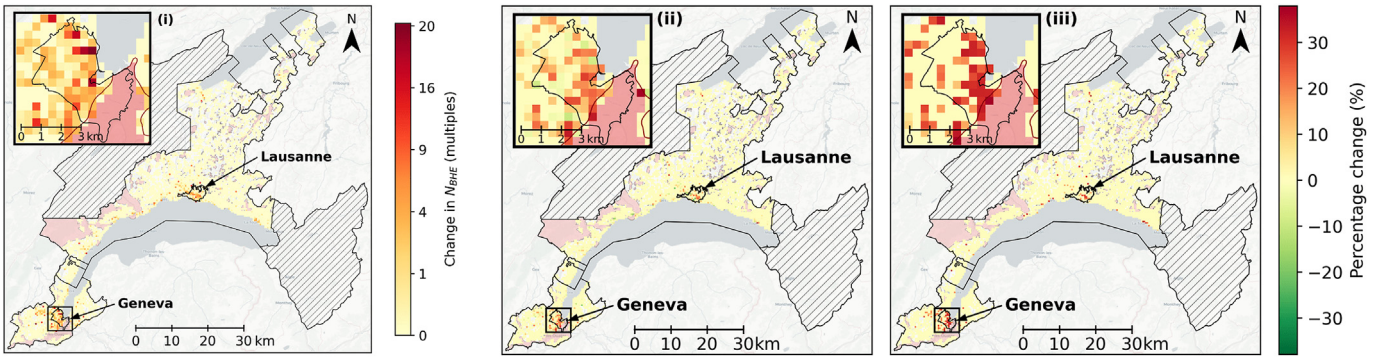

Fig. 6. Change in number of boreholes N_{BHE} (a), heat extraction rate q_{max} (b) and heating operating time $t_{op,h}$ (c) of the partial cooling scenario (PC-ND-4.5) compared to the baseline (NC-ND), computed as the difference between the two scenarios divided by the baseline. The change in N_{BHE} is shown as multiples on a quadratic scale.

Table 5
Mean and 95% confidence intervals of the technical heat exchange potential (heat injection and heat extraction) summed over the case study area for all scenarios, based on Monte Carlo simulation.

Scenario	Heat injection Q_{inj} (TWh/y)			Heat extraction Q_{extr} (TWh/y)		
Base scenario	0			4.64		
PC-ND	0.99 ± 0.10	1.15 ± 0.12	1.30 ± 0.13	5.56 ± 0.09	5.70 ± 0.10	5.84 ± 0.12
FC-ND	1.93 ± 0.15	2.21 ± 0.17	2.46 ± 0.34	6.42 ± 0.13	6.67 ± 0.15	6.89 ± 0.38
PC-D	1.35 ± 0.14	1.60 ± 0.17	1.85 ± 0.19	5.90 ± 0.13	6.12 ± 0.15	6.34 ± 0.17
FC-D	2.78 ± 0.23	3.24 ± 0.27	3.69 ± 0.30	7.18 ± 0.20	7.59 ± 0.23	7.98 ± 0.26
Climate model	*RCP 2.6*	*RCP 4.5*	*RCP 8.5*	*RCP 2.6*	*RCP 4.5*	*RCP 8.5*

Table 6
Useful potential to supply building heating and cooling demands in scenarios without DHC.

Scenario	Useful cooling potential Q_{cool} (TWh/y)			Useful heating potential Q_{heat} (TWh/y)		
Base scenario	0			2.19 (35%)		
PC-ND	0.84 (63%)	0.97 (62%)	1.10 (60%)	2.90 (47%)	2.96 (48%)	3.02 (49%)
FC-ND	1.63 (60%)	1.87 (59%)	2.08 (57%)	3.26 (53%)	3.32 (54%)	3.37 (55%)
Climate model	*RCP 2.6*	*RCP 4.5*	*RCP 8.5*	*RCP 2.6*	*RCP 4.5*	*RCP 8.5*

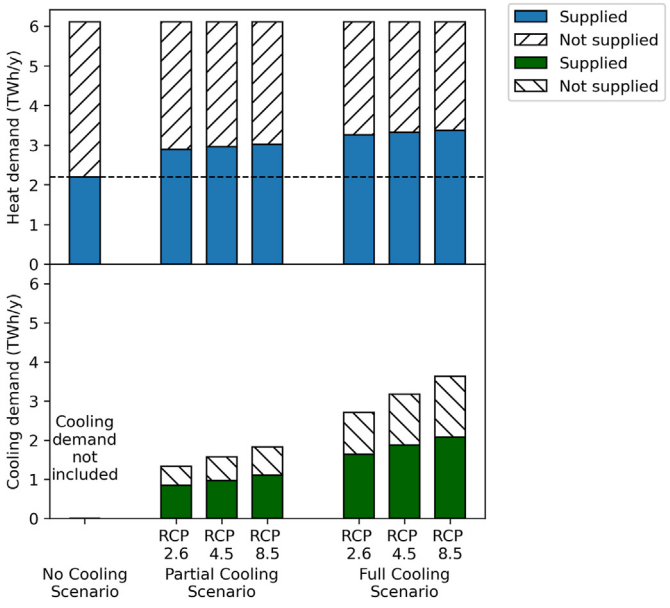

Fig. 8. Supply of building heating and cooling demands in scenarios without DHC.

space cooling demand could be supplied by GSHPs while increasing the useful potential for supplying heat demand by 0.7–0.8 TWh. Similarly, in the FC-ND scenario, GSHPs could meet 1.6–2.0 TWh building cooling demand, as well as supply additional 1.1–1.2 TWh to building heating demand. The fraction of demand covered (values in brackets) is nearly constant across the three climate models for all scenarios, which suggests a high robustness of the results to climate change.

Fig. 9 shows maps of the heat and cooling supply in percentage for the PC-ND-4.5 scenario as an example. In the case of supplying cooling (Fig. 9a), we found that building cooling demand could be sufficiently supplied where GSHP installation is allowed, due to the high capacity of BHEs to inject excess heat from space cooling. By contrast, no cooling demand can be supplied in areas where GSHP installation is prohibited (see insets in Fig. 9a). In the case of supplying heat (Fig. 9b), despite an increased potential due to seasonal regeneration, heat demand is not sufficiently supplied in dense urban areas with an excessive demand density. Although the technical potential is abundant in low-density areas, it is not available to other areas with a deficit, due to spatial constraints. In addition, constraints on GSHP installation further limit the heat supply (see Fig. 3b).

4.3. Impact of district heating and cooling

The integration of GSHPs in DHC increases the useful potential to supply heating and cooling demand by at least 22 percentage points compared to the results presented in Section 4.2. As shown in Table 7, the utilization of DHC improves the useful potential in all seven scenarios with DHC, which are again robust to the climate models. The amount of energy supplied within DHC increases as more heat is re-injected to the ground, due to the high demand in dense areas (see Fig. 10). These results demonstrate the two-fold benefit of DHC: First, more injection of space cooling demand results in an increased technical potential. Second, DHC eases the spatial constraints for the useful potential for heating and allows integrating more surplus geothermal energy in neighbouring areas as potential supply sources of the DHC.

To illustrate the impact of DHC at regional scale, Fig. 11 shows maps of the change in heating and cooling supply between PC-ND-4.5 and PC-D-4.5 scenarios as an example. In the case of cooling (Fig. 11a), the utilization of DHC allows the distribution of cooling energy from GSHPs to buildings located in areas where GSHP installation is prohibited (see inset (i) in Fig. 11a). In the case of heat supply (Fig. 11b), DHC could largely improve the insufficient supply in dense urban areas.

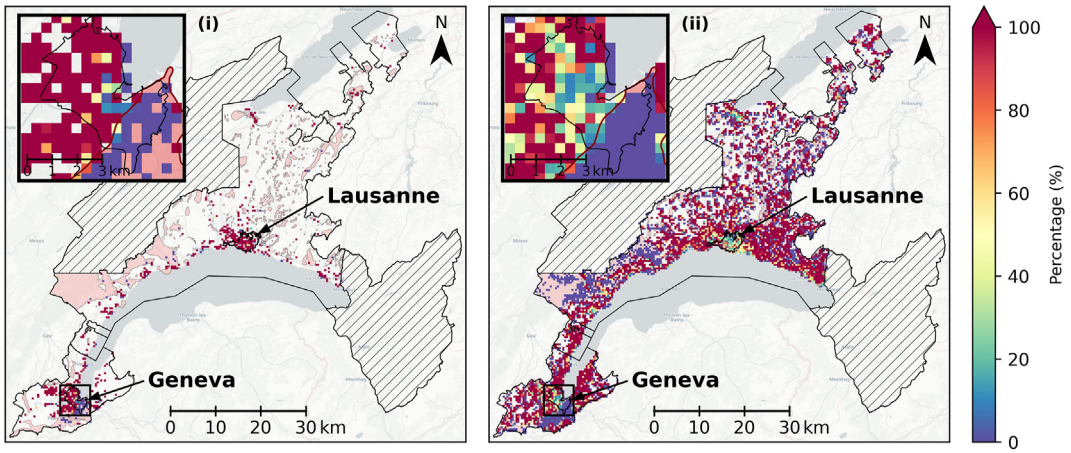

Fig. 9. Distribution of demand coverage per pixel in the PC-ND-4.5 scenario: (a) percentage of cooling demand supplied; (b) percentage of heat demand supplied.

Table 7
Useful potential to supply building heating and cooling demands in scenarios with DHC.

Scenarios	Useful cooling potential Q_{cool} (TWh/y)			Useful heat potential Q_{heat} (TWh/y)		
NC-D	0			3.86 (63%)		
PC-D	1.14 (86%)	1.35 (86%)	1.57 (86%)	4.20 (69%)	4.44 (73%)	4.60 (75%)
FC-D	2.35 (87%)	2.74 (86%)	3.13 (86%)	5.07 (83%)	5.15 (84%)	5.20 (85%)
Climate model	*RCP 2.6*	*RCP 4.5*	*RCP 8.5*	*RCP 2.6*	*RCP 4.5*	*RCP 8.5*

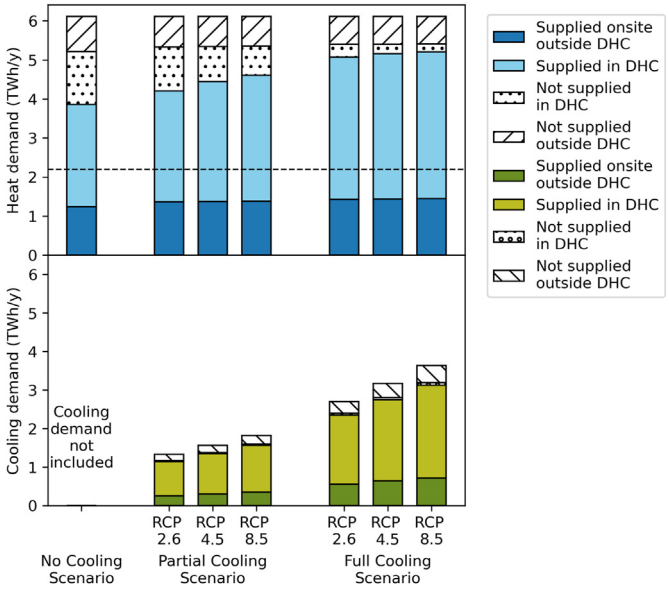

Fig. 10. Supply of building heating and cooling demands in scenarios with DHC.

5. Discussion

5.1. Methodological contribution

This paper proposes a novel framework to estimate the technical and useful potential of shallow GSHPs for building heating and cooling in individual GSHP systems and in DHC, which scalable to entire regions. For the first time, this framework combines (i) the spatial mapping between heat demands and virtually installed BHEs, (ii) the analytical modelling of the technical heat exchange potential from bi-directional GSHPs, considering seasonal regeneration through the re-injection of space cooling demands, and (iii) the optimal allocation of potential heat sources within DHC. The analytical model, which is built upon previous work on the heat extraction potential from GSHPs [23], to account for (i) technical constraints due to the combined heat injection and extraction, and (ii) different operating strategies of GSHP systems. The advantages of the proposed method are that it (i) accounts for thermal interactions between densely installed GSHPs and the seasonal variation of the energy demand, (ii) proposes a trade-off between operating power and heat exchange potential, and (iii) is scalable to thousands of borehole fields.

We further expanded previous work on the identification of potential DHC areas [52] by introducing a graph-theory based optimization to match building thermal energy demand to technical geothermal potential. This approach permits to quantify the impact of DHC on the useful geothermal potential. The proposed method is transferable to other heat sources for seasonal regeneration, such as solar thermal generation, waste heat or air-source heat pumps [72]. The framework may also be replicated in other regions within or outside of Switzerland. Many of the required regional input data are available at European scale or beyond, or can be mapped from the literature using existing methods. An overview of these datasets and mapping approaches, which assure the replicability beyond the case study, are provided in Appendix B.

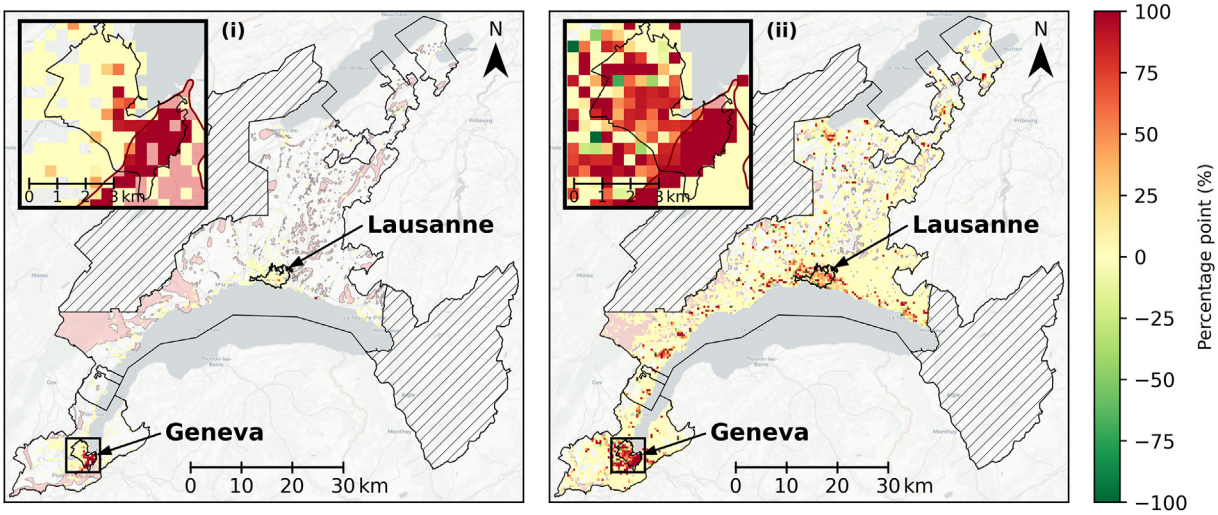

Fig. 11. The difference between PC-ND-4.5 and PC-D-4.5 scenarios: a) percentage of cooling demand supplied; b) percentage of heat demand supplied.

5.2. Practical implications and application

The results of the case study in the Swiss cantons of Vaud and Geneva imply that seasonal regeneration of GSHP systems may significantly increase the potential heat extraction. We found that the re-injection of space cooling demands into the ground allows for maximum annual heat extraction densities above 300 kWh/m^2 at heat injection densities above 330 kWh/m^2, especially in centres of large urban areas. The comparison of shallow geothermal potential studies by Bayer et al. [18] indicates that the maximum energy densities correspond to the yields of boreholes with little or no thermal interference [34,73]. We also found that the maximum technical potential is consistent with a previous Swiss case study for a commercial GSHP installation [46], which suggests a heat extraction density of 440 kWh/m^2 at 610 kWh/m^2 of heat injection. Across the case study region, the heat extraction potential increases with the amount of cooling injection from 4.6 TWh without regeneration up to 6.9 TWh. The spatial resolution of pixels of (400×400) m^2 highlights regional differences of the shallow geothermal potential between rural, suburban and urban areas.

We further estimate that the conversion rate of injected to additional extracted heat is 90%, showing the high impact of seasonal regeneration on reducing thermal interference. Integrating GSHPs within DHC increases the fraction of the building thermal demand supplied through geothermal energy by up to 30 percentage points for both heating and cooling. The fractions are nearly independent of different climate change scenarios for 2050, which implies robustness towards uncertainties in future climate. Low confidence intervals across 2000 Monte Carlo runs also suggest that the spatial distribution of the cooling demand has a low impact on the total potential.

The results may be applied to identify strategic areas for installing GSHPs in individual and district heating systems. This work can further be used as a basis for economic studies to compare the cost-effectiveness of renewable energy sources, therefore helping to design future energy systems. Finally, the findings presented above may provide useful input for policy makers to discuss the regional and national renewable energy strategies.

5.3. Limitations and future work

Quantifying the impact of seasonal regeneration of GSHPs is subject to assumptions and limitations related to the data and the modelling approach. The main assumptions and limitations related to data are that (i) all potential GSHP systems and energy demands within each pixel of 400 × 400 m^2 are connected. This assumption is necessary to assure the scalability of the approach; (ii) for each potential DHC area, all GSHP systems and buildings are connected to the same DHC. Any GSHP system adjacent to DHC areas is a potential further heat source; (iii) the mapping of geothermal potential to building energy demands is done by calculating heat balances. DHC network topologies, operating temperatures and thermal losses are not addressed; and (iv) we consider only the space cooling demand in the service sector. Space cooling in the residential sector is not modelled, as the proportion of expected residential space cooling demand for 2050 is small (5%–35%) according to forecasts for neighbouring countries [74].

The key assumptions of the analytical model, which are described in detail in Ref. [23], are that (i) the impact of groundwater flow on the technical geothermal potential is neglected, due to a lack of available data. Groundwater flow may impact both the magnitude of the GSHP potential and the direction of thermal interferences, which we assumed to be isotropic in all directions; (ii) the GSHP systems use the full available area and are designed such as to provide the estimated heat extraction rate and annual energy; and (iii) all systems start the heat extraction simultaneously, neglecting any previously existing systems.

Future work is needed to assess the technical barriers for using shallow geothermal energy in future DHC and to account for the impact of groundwater flow on the technical potential. Furthermore, environmental consequences of long-term warming or cooling trends of the ground related to the net injection or extraction of heat may be investigated. To adapt the method to country scale, statistical methods such as Machine Learning may be used. The method proposed here may also be used to model other systems for seasonal regeneration at large scale, such as the re-injection of excess solar thermal generation. This study can be used as the basis for further work to explore the economic and emission reduction potential of shallow geothermal combined with district heating and cooling. Such further work may also address the potential of hybrid GSHPs with other heat sources such as industrial waste heat or solar thermal generation, as well as complementarities with renewable electricity generation from wind turbines or solar photovoltaics.

6. Conclusion

This work presents a novel framework to estimate the technical and useful potential of shallow ground-source heat pumps (GSHPs) to supply building heating and cooling demands at regional scale. The framework accounts for the geospatial matching of heat demands and potential GSHP systems, the modelling of technical potential with seasonal regeneration of GSHPs through re-injection of excess heat from space cooling, and for the optimal allocation of heat supply in district heating and cooling (DHC). The useful potential is obtained for the direct heat exchange between buildings and geothermal fields and by considering DHC. A scenario-based approach is used to assess the technical and useful geothermal potential under different climate change scenarios, market penetration levels of cooling systems, and the possible use of DHC.

The case study in western Switzerland suggests that seasonal regeneration may significantly reduce thermal interference between boreholes. This increases the maximum technical geothermal potential density from 15 kWh/m^2 without heat injection to above 300 kWh/m^2 in pixels with heat injection densities above 330 kWh/m^2. These values are consistent with results reported in related scientific literature and case studies of existing installations. Results further suggest that the useful geothermal potential may cover up to 63% of service-sector cooling demand and up to 55% of heat demand in 2050 (assumed at 50% of current heat demand) for individual GSHP systems in western Switzerland, which increases to 87% and 85% if DHC is used. The results are robust to uncertainties in future climate. The outcomes of the study may be used to conduct techno-economic analyses of future energy systems with a high share of renewable heat generation and to inform decision-making aimed at achieving Switzerland's renewable energy targets for 2050.

Credit author statement

Alina Walch & Xiang Li: Conceptualization, Methodology, Software, Visualization, Writing - Original draft. **Jonathan**

Chambers Conceptualization, Methodology, Writing - Review & Editing, Supervision. **Selin Yilmaz:** Writing - Review & Editing, Supervision. **Nahid Mohajeri:** Conceptualization, Writing - Review & Editing, Supervision, Funding acquisition. **Jean-Louis Scartezzini & Martin Patel:** Supervision, Project administration, Funding acquisition.

Declaration of competing interest

The authors declare that they have no known competing financial interests or personal relationships that could have appeared to influence the work reported in this paper.

Acknowledgements

We thank the reviewers and the editor for thorough reviews and helpful comments on an earlier version of this article. This research has been financed partly by the Swiss Innovation Agency Innosuisse under the Swiss Competence Center for Energy Research SCCER FEEB&D, partly by the Swiss Federal Office of Energy (SFOE) under the project SWiss Energy research for the Energy Transition (SWEET) DeCarbCH and partly by the Swiss National Science Foundation (SNSF) under the National Research Program 75 (Big Data).

Appendix A. Heating and cooling degree days

The heating and cooling degree days (HDD/CDD) are computed from daily mean ambient temperature (T_{amb}) [75]. For HDD, we use the formula provided in the Swiss norm SIA 2028 [70]:

$$HDD = \sum_{\mathrm{d}=1}^{\mathrm{d_m}} (20°\mathrm{C} - \mathrm{T}_{amb}(\mathrm{d},\mathrm{m})) \quad \forall \mathrm{T}_{amb}(\mathrm{d},\mathrm{m}) \leq 12°C \tag{A.1}$$

where d, m denote the day and month and d_m is the number of days in each month. As no Swiss norm exists for CDD, we obtain the CDD from Ref. [75] using a reference temperature of 18°C:

$$CDD = \sum_{\mathrm{d}=1}^{\mathrm{d_m}} (\mathrm{T}_{amb}(\mathrm{d},\mathrm{m}) - 18°\mathrm{C}) \quad \forall \mathrm{T}_{amb}(\mathrm{d},\mathrm{m}) \geq 18°\mathrm{C} \tag{A.2}$$

The maximum monthly heating/cooling weights ($w_{hdd/cdd,\,max}$) are obtained as [23]:

$$w_{hdd/cdd,\,max} = 1.05\,\frac{HDD/CDD_{max}}{\sum HDD/CDD} \tag{A.3}$$

where the HDD/CDD_{max} are the maximum monthly HDD/CDD.

Appendix B. Data availability beyond the case study area

To replicate the proposed methods outside of the case study area, the input datasets summarized in Table 1 must be obtained for the area of interest. While many of the required input datasets are available at European scale or beyond, other datasets would have to be approximated. Notably, maps of the thermal ground properties are rarely available. For large-scale studies, these can be mapped from literature data based on geological characteristics, as performed for example in Refs. [11,14,76,77]. Such mapping is a crude approximation, and the results must be interpreted in this context. However, related work has shown that the thermal ground properties are not the most important features impacting GSHP performance [78], so this approach may be acceptable for large-scale studies.

Furthermore, the quality and resolution of the input data have to be suitable for the target application. The proposed analytical model is applied at individual parcel scale, which can be derived for example from OpenStreetMap data. For analyses at country scale or at pan-European scale, for example, even low-resolution inputs, for example using heat demand pixels at km-scale, may be acceptable for the replication of the proposed framework. At city scale, data is often available at higher quality and higher spatial resolution, allowing to obtain more accurate results. An overview of the required input datasets, there potential availability in the European context and suggestions of references are provided in Table B.1.

Table B.1
Suggestions of methods and datasets to obtain the required input data for the replicability of the proposed framework beyond the case study region. References are provided for the European scale where possible, but they are not exhaustive.

	Input dataset	Potential availability	References (Europe)
Spatial constraints	Available area for BHEs	Can be obtained from national topographic data or OpenStreetMap (OSM) following the method in [23]	OSM [79]
	DHC zones	Can be obtained from the Heat Roadmap Europe[1] or derived using the method proposed in [67]	Heat Roadmap Europe [80]
	GSHP restrictions	Can be neglected for a rough potential estimate, or estimated from national hydrogeological data	SwissTopo [81] (Switzerland)
Geothermal input data	Thermal ground properties	If no 3D underground models or measurements are available, mapping of literature values to geological data may be performed in analogy to related studies [11,14,76,77]	SIA [45], VDI [82]
	Surface temperature	Can be derived from air temperature (see below) following [45,83]	COSMO[2]
	Air temperature	Reanalysis (e.g. COSMO REA) or other gridded data can be used	
	Full-load heating hours	Can be obtained from literature/norms	SIA [45], Kavanaugh [48]
Building energy demands	Building heating demand	Can be obtained from the Heat Roadmap Europe[1] for the reference year 2015. Future penetration of cooling equipment must be assessed in further work.	Heat Roadmap Europe [84], Hotmaps [85]
	Building cooling demand		Heat Roadmap Europe [86]

[1] https://heatroadmap.eu/peta4/.
[2] https://reanalysis.meteo.uni-bonn.de/.

Research data for this article

The research data related to this article is available at: https://doi.org/10.5281/zenodo.5575318.

References

[1] Lund JW, Toth A. "Direct utilization of geothermal energy 2020 worldwide review," presented at the world geothermal congress, reykjavik. May 2020. Iceland.
[2] Florides G, Kalogirou S. Ground heat exchangers—a review of systems, models and applications. Renew Energy Dec. 2007;32(15):2461–78. https://doi.org/10.1016/j.renene.2006.12.014.
[3] Santamouris M. Cooling the buildings – past, present and future. Energy Build Sep. 2016;128:617–38. https://doi.org/10.1016/j.enbuild.2016.07.034.
[4] Soltani M, et al. A comprehensive study of geothermal heating and cooling systems. Sustain Cities Soc Jan. 2019;44:793–818. https://doi.org/10.1016/j.scs.2018.09.036.
[5] Vienken T, Kreck M, Dietrich P. Monitoring the impact of intensive shallow geothermal energy use on groundwater temperatures in a residential neighborhood. Geoth Energy Mar. 2019;7(1):8. https://doi.org/10.1186/s40517-019-0123-x.
[6] Hähnlein S, Bayer P, Ferguson G, Blum P. Sustainability and policy for the thermal use of shallow geothermal energy. Energy Pol Aug. 2013;59:914–25. https://doi.org/10.1016/j.enpol.2013.04.040.
[7] Werner S. International review of district heating and cooling. Energy Oct. 2017;137:617–31. https://doi.org/10.1016/j.energy.2017.04.045.
[8] Lund H, et al. 4th Generation District Heating (4GDH). Integrating smart thermal grids into future sustainable energy systems. Energy 2014;68:1–11. https://doi.org/10.1016/j.energy.2014.02.089.
[9] Garabetian T, et al. EGEC geothermal market report. ninth ed. " EGEC - European Geothermal Energy Council; Jun. 2020.
[10] Casasso A, Sethi R. Assessment and mapping of the shallow geothermal potential in the province of Cuneo (Piedmont, NW Italy). Renew Energy Mar. 2017;102:306–15. https://doi.org/10.1016/j.renene.2016.10.045.
[11] Galgaro A, et al. Empirical modeling of maps of geo-exchange potential for shallow geothermal energy at regional scale. Geothermics Sep. 2015;57:173–84. https://doi.org/10.1016/j.geothermics.2015.06.017.
[12] García-Gil A, et al. GIS-supported mapping of low-temperature geothermal potential taking groundwater flow into account. Renew Energy May 2015;77:268–78. https://doi.org/10.1016/j.renene.2014.11.096.
[13] Muñoz M, et al. Estimating low-enthalpy geothermal energy potential for district heating in Santiago basin—Chile (33.5 °S). Renew Energy Apr. 2015;76:186–95. https://doi.org/10.1016/j.renene.2014.11.019.
[14] Perego R, Pera S, Galgaro A. Techno-economic mapping for the improvement of shallow geothermal management in southern Switzerland. Energies Jan. 2019;12(2):279. https://doi.org/10.3390/en12020279.
[15] Tissen C, Menberg K, Bayer P, Blum P. Meeting the demand: geothermal heat supply rates for an urban quarter in Germany. Geoth Energy Dec. 2019;7(1):9. https://doi.org/10.1186/s40517-019-0125-8.
[16] Zhang Y, Soga K, Choudhary R. Shallow geothermal energy application with GSHPs at city scale: study on the City of Westminster. Géotech Lett Apr. 2014;4(2):125–31. https://doi.org/10.1680/geolett.13.00061.
[17] Miglani S, Orehounig K, Carmeliet J. A methodology to calculate long-term shallow geothermal energy potential for an urban neighbourhood. Energy Build 2018;159:462–73. https://doi.org/10.1016/j.enbuild.2017.10.100.
[18] Bayer P, Attard G, Blum P, Menberg K. The geothermal potential of cities. Renew Sustain Energy Rev May 2019;106:17–30. https://doi.org/10.1016/j.rser.2019.02.019.
[19] Rivera JA, Blum P, Bayer P. Increased ground temperatures in urban areas: estimation of the technical geothermal potential. Renew Energy Apr. 2017;103:388–400. https://doi.org/10.1016/j.renene.2016.11.005.
[20] Fascì ML, Lazzarotto A, Acuna J, Claesson J. Analysis of the thermal interference between ground source heat pump systems in dense neighborhoods. Sci Technol Built Environ Sep. 2019;25(8):1069–80. https://doi.org/10.1080/23744731.2019.1648130.
[21] Attard G, Bayer P, Rossier Y, Blum P, Eisenlohr L. A novel concept for managing thermal interference between geothermal systems in cities. Renew Energy Jan. 2020;145:914–24. https://doi.org/10.1016/j.renene.2019.06.095.
[22] Alcaraz M, Vives L, Vázquez-Suñé E. The T-I-GER method: a graphical alternative to support the design and management of shallow geothermal energy exploitations at the metropolitan scale. Renew Energy Aug. 2017;109:213–21. https://doi.org/10.1016/j.renene.2017.03.022.
[23] Walch A, Mohajeri N, Gudmundsson A, Scartezzini J-L. Quantifying the technical geothermal potential from shallow borehole heat exchangers at regional scale. Renew Energy Mar. 2021;165:369–80. https://doi.org/10.1016/j.renene.2020.11.019.
[24] Wagner R, Weisskopf T. Erdsondenpotenzial in der Stadt zürich. Schlussbericht: " Amt für Hochbauten Stadt Zürich; 2014.
[25] Kriesi R. Methoden der Erdsonden-Regeneration mit Sekundärnutzen oder tiefen Wärmekosten. Schlussbericht: " Amt für Hochbauten Stadt Zürich; 2017.
[26] Miglani S, Orehounig K, Carmeliet J. Integrating a thermal model of ground source heat pumps and solar regeneration within building energy system optimization. Appl Energy May 2018;218:78–94. https://doi.org/10.1016/j.apenergy.2018.02.173.
[27] Liu Z, Xu W, Zhai X, Qian C, Chen X. Feasibility and performance study of the hybrid ground-source heat pump system for one office building in Chinese heating dominated areas. Renew Energy Feb. 2017;101:1131–40. https://doi.org/10.1016/j.renene.2016.10.006.
[28] Pahud D. A case study: the dock midfield of zurich airport. In: Energy geostructures. John Wiley & Sons, Ltd; 2013. p. 281–96. https://doi.org/10.1002/9781118761809.ch14.
[29] Girard A, Gago EJ, Muneer T, Caceres G. Higher ground source heat pump COP in a residential building through the use of solar thermal collectors. Renew Energy Aug. 2015;80:26–39. https://doi.org/10.1016/j.renene.2015.01.063.
[30] Michopoulos A, Papakostas KT, Kyriakis N. Potential of autonomous ground-coupled heat pump system installations in Greece. Appl Energy Jun. 2011;88(6):2122–9. https://doi.org/10.1016/j.apenergy.2010.12.061.
[31] Aditya GR, Narsilio GA. Environmental assessment of hybrid ground source heat pump systems. Geothermics Sep. 2020;87:101868. https://doi.org/10.1016/j.geothermics.2020.101868.
[32] Nguyen HV, Law YLE, Alavy M, Walsh PR, Leong WH, Dworkin SB. An analysis of the factors affecting hybrid ground-source heat pump installation potential in North America. Appl Energy Jul. 2014;125:28–38. https://doi.org/10.1016/j.apenergy.2014.03.044.
[33] Rad FM, Fung AS, Leong WH. Feasibility of combined solar thermal and ground source heat pump systems in cold climate, Canada. Energy Build Jun. 2013;61:224–32. https://doi.org/10.1016/j.enbuild.2013.02.036.
[34] Casasso A, Sethi R. G . pot : a quantitative method for the assessment and mapping of the shallow geothermal potential. Energy 2016;106:765–73. https://doi.org/10.1016/j.energy.2016.03.091.
[35] Schiel K, Baume O, Caruso G, Leopold U. GIS-based modelling of shallow geothermal energy potential for CO 2 emission mitigation in urban areas. Renew Energy 2016;86:1023–36. https://doi.org/10.1016/j.renene.2015.09.017.
[36] Kljajić MV, Anđelković AS, Hasik V, Munćan VM, Bilec M. Shallow geothermal energy integration in district heating system: an example from Serbia. Renew Energy Mar. 2020;147:2791–800. https://doi.org/10.1016/j.renene.2018.11.103.
[37] Jensen JK, Ommen T, Markussen WB, Elmegaard B. Design of serially connected district heating heat pumps utilising a geothermal heat source. Energy Oct. 2017;137:865–77. https://doi.org/10.1016/j.energy.2017.03.164.
[38] Alberg Østergaard P, Mathiesen BV, Möller B, Lund H. A renewable energy scenario for Aalborg Municipality based on low-temperature geothermal heat, wind power and biomass. Energy Dec. 2010;35(12):4892–901. https://doi.org/10.1016/j.energy.2010.08.041.
[39] Carotenuto A, Figaj RD, Vanoli L. A novel solar-geothermal district heating, cooling and domestic hot water system: dynamic simulation and energy-economic analysis. Energy Dec. 2017;141:2652–69. https://doi.org/10.1016/j.energy.2017.08.084.
[40] Formhals J, Feike F, Hemmatabady H, Welsch B, Sass I. Strategies for a transition towards a solar district heating grid with integrated seasonal geothermal energy storage. Energy Aug. 2021;228:120662. https://doi.org/10.1016/j.energy.2021.120662.
[41] Unternährer J, Moret S, Joost S, Maréchal F. Spatial clustering for district heating integration in urban energy systems: application to geothermal energy. Appl Energy Mar. 2017;190:749–63. https://doi.org/10.1016/j.apenergy.2016.12.136.
[42] Lund R, Persson U. Mapping of potential heat sources for heat pumps for district heating in Denmark. Energy Sep. 2016;110:129–38. https://doi.org/10.1016/j.energy.2015.12.127.
[43] Stegnar G, et al. A framework for assessing the technical and economic potential of shallow geothermal energy in individual and district heating systems: a case study of Slovenia. Energy Aug. 2019;180:405–20. https://doi.org/10.1016/j.energy.2019.05.121.
[44] Blum A, Wyss R. Statistik der geothermischen Nutzung in der Schweiz – ausgabe 2016. Switzerland: EnergieSchweiz, Bern; 2016.
[45] SIA. Sondes géothermiques (SIA384/6). Swiss Society of Engineers and Architects; 2010.
[46] Pahud D. Geothermal energy and heat storage. Switzerland: SUPSI Laboratory of Energy, Ecology and Economy; 2002.
[47] Eskilson P. Thermal analysis of heat extraction boreholes. Sweden: University of Lund; 1987.
[48] Kavanaugh S, Rafferty K. Geothermal heating and cooling: design of ground-source heat pump systems. ASHRAE; 2014. Mar. 23, 2020. [Online]. Available: https://www.ashrae.org/technical-resources/bookstore/geothermal-heating-and-cooling-design-of-ground-source-heat-pump-systems.
[49] Alavy M, Dworkin SB, Leong WH. A design methodology and analysis of combining multiple buildings onto a single district hybrid ground source heat pump system. Renew Energy Jun. 2014;66:515–22. https://doi.org/10.1016/j.renene.2013.12.030.
[50] Sarbu I, Sebarchievici C. General review of ground-source heat pump systems for heating and cooling of buildings. Energy Build Feb. 2014;70:441–54. https://doi.org/10.1016/j.enbuild.2013.11.068.
[51] Foster S, Love J, Walker I, Crane M. Heat pumps in district heating. Final report. *Department of Energy & Climate Change*; 2016.
[52] Chambers J, Zuberi S, Jibran M, Narula K, Patel MK. Spatiotemporal analysis of

industrial excess heat supply for district heat networks in Switzerland. Energy 2020;192:116705. https://doi.org/10.1016/j.energy.2019.116705.
[53] Li X, Walch A, Yilmaz S, Patel MK, Chambers J. Optimal spatial resource allocation in networks: application to district heating and cooling. *Submitted to Computers & Industrial Engineering*; 2021.
[54] Hitchcock FL. The distribution of a product from several sources to numerous localities. J Math Phys 1941;20(1–4):224–30. https://doi.org/10.1002/sapm1941201224.
[55] Dantzig GB. Linear programming and extensions, vol. 48. Princeton university press; 1998. Dec. 03, 2020. [Online]. Available: https://press.princeton.edu/books/paperback/9780691059136/linear-programming-and-extensions.
[56] Mohajeri N, Perera ATD, Coccolo S, Mosca L, Le Guen M, Scartezzini J-L. Integrating urban form and distributed energy systems: assessment of sustainable development scenarios for a Swiss village to 2050. Renew Energy Dec. 2019;143:810–26. https://doi.org/10.1016/j.renene.2019.05.033.
[57] Frank Th. Climate change impacts on building heating and cooling energy demand in Switzerland. Energy Build Nov. 2005;37(11):1175–85. https://doi.org/10.1016/j.enbuild.2005.06.019.
[58] IPPC. Climate change 2014: synthesis report. Contribution of working groups I, II and III to the fifth assessment report of the intergovernmental Panel on climate change. Geneva, Switzerland: IPCC; 2014.
[59] ASIT VD. Cadastre - MO et NPCS - thème Biens-fonds. www.asitvd.ch/md/03d4716b-66af-f4d4-99a2-83406987ad32. [Accessed 22 January 2020].
[60] SITG. Parcelles de la mensuration. https://ge.ch/sitg/fiche/8450. [Accessed 23 March 2020].
[61] Swisstopo, "swissTLM3D Version 1.6," Swisstopo, Nachführungsinfo 2018, 2018. [Online]. Available: https://shop.swisstopo.admin.ch/de/products/landscape/tlm3D.
[62] ASIT VD. Cadastre de géothermie basse température. Feb. 04, 2020, www.asitvd.ch/md/f8c427d3-dc9e-4864-c593-f763b122e824; Mar. 12, 2019.
[63] SITG. GEOTHERMIE (Groupe). Jun. 23, 2021. https://ge.ch/sitg/fiche/1006. 19, October 2021.
[64] Assouline D, Mohajeri N, Gudmundsson A, Scartezzini J-L. A machine learning approach for mapping the very shallow theoretical geothermal potential. Geoth Energy Dec. 2019;7(1):19. https://doi.org/10.1186/s40517-019-0135-6.
[65] MeteoSwiss. "Daily mean, minimum and maximum temperature," federal office of meteorology and climatology MeteoSwiss, documentation of MeteoSwiss grid-data products. 2017.
[66] Swisstopo. swissALTI3D - the high precision digital elevation model of Switzerland. https://shop.swisstopo.admin.ch/en/products/height_models/alti3D. [Accessed 13 August 2019].
[67] Chambers J, Narula K, Sulzer M, Patel MK. Mapping district heating potential under evolving thermal demand scenarios and technologies: a case study for Switzerland. Energy Jun. 2019;176:682–92. https://doi.org/10.1016/j.energy.2019.04.044.
[68] Schneider S, Hollmuller P, Le Strat P, Khoury J, Patel M, Lachal B. Spatial–temporal analysis of the heat and electricity demand of the Swiss building stock. Front Built Environ Aug. 2017;3:53. https://doi.org/10.3389/fbuil.2017.00053.
[69] Li X, Chambers J, Yilmaz S, Patel MK. A Monte Carlo building stock model of space cooling demand in the Swiss service sector under climate change. Energy Build Dec. 2020:110662. https://doi.org/10.1016/j.enbuild.2020.110662.
[70] SIA. Klimadaten für Bauphysik, Energie- und Gebäudetechnik (SIA 2028). Swiss Society of Engineers and Architects; 2010.
[71] BFE. Energiestrategie 2050: erstes massnahmenpaket. Switzerland: Bundesamt für Energie BFE; 2012.
[72] Kim Y, Lee JS, Jeon SW. Hybrid ground-source heat pump systems. In: Advances in ground-source heat pump systems. Elsevier; 2016. p. 331–57. https://doi.org/10.1016/B978-0-08-100311-4.00012-1.
[73] Ondreka J, Rüsgen MI, Stober I, Czurda K. GIS-supported mapping of shallow geothermal potential of representative areas in south-western Germany—possibilities and limitations. Renew Energy Oct. 2007;32(13):2186–200. https://doi.org/10.1016/j.renene.2006.11.009.
[74] Paardekooper S, et al. Heat roadmap Europe 4: quantifying the impact of low-carbon heating and cooling roadmaps. *Aalborg Universitetsforlag.*; Oct. 2018. Jul. 22, 2021. [Online]. Available: https://vbn.aau.dk/en/publications/heat-roadmap-europe-4-quantifying-the-impact-of-low-carbon-heatin.
[75] Christenson M, Manz H, Gyalistras D. Climate warming impact on degree-days and building energy demand in Switzerland. Energy Convers Manag Apr. 2006;47(6):671–86. https://doi.org/10.1016/j.enconman.2005.06.009.
[76] Casasso A, Sethi R, "Pot G. A quantitative method for the assessment and mapping of the shallow geothermal potential. Energy Jul. 2016;106:765–73. https://doi.org/10.1016/j.energy.2016.03.091.
[77] Gemelli A, Mancini A, Longhi S. GIS-based energy-economic model of low temperature geothermal resources: a case study in the Italian Marche region. Renew Energy Sep. 2011;36(9):2474–83. https://doi.org/10.1016/j.renene.2011.02.014.
[78] Walch A, Castello R, Mohajeri N, Gudmundsson A, Scartetzzini J-L. Using Machine Learning to estimate the technical potential of shallow ground-source heat pumps with thermal interference. Lausanne, Switzerland: presented at the CISBAT 2021; 2021.
[79] OpenStreetMap Wiki. Elements. https://wiki.openstreetmap.org/wiki/Elements; 2021.
[80] Möller B, Persson U. Updated Peta atlas for each MS with the final level of district heating recommended in WP6. Heat Roadmap Eur Deliv 2018;6.
[81] swisstopo, "GeoMaps 500 - Vector," *Federal Office of Topography swisstopo*. https://www.swisstopo.admin.ch/en/geodata/geology/maps/gk500/vector.html (accessed Jun. 22, 2021).
[82] VDI, VDI 4640 Blatt 2. Thermische Nutzung des Untergrunds - erdgekoppelte Wärmepumpenanlagen. Verein Deutscher Ingenieure. Jun. 19, 2021. [Online]. Available: https://www.vdi.de/richtlinien/details/vdi-4640-blatt-2-thermische-nutzung-des-untergrunds-erdgekoppelte-waermepumpenanlagen; 2019.
[83] Signorelli S, Kohl T. Regional ground surface temperature mapping from meteorological data. Global Planet Change Feb. 2004;40(3):267–84. https://doi.org/10.1016/j.gloplacha.2003.08.003.
[84] Möller B, Wiechers E, Persson U, Grundahl L, Connolly D. Heat Roadmap Europe: identifying local heat demand and supply areas with a European thermal atlas. Energy Sep. 2018;158:281–92. https://doi.org/10.1016/j.energy.2018.06.025.
[85] Müller A, Hummel M, Kranzl L, Fallahnejad M, Büchele R. Open source data for gross floor area and heat demand density on the hectare level for EU 28. Energies Jan. 2019;12(24). https://doi.org/10.3390/en12244789. Art. no. 24.
[86] Werner S. European space cooling demands. Energy Sep. 2016;110:148–56. https://doi.org/10.1016/j.energy.2015.11.028.